EXPERIMENTAL INVESTIGATIONS OF HYDROGEN CLUSTER IONS

H. A. VAN LUMIG

EXPERIMENTAL INVESTIGATIONS OF HYDROGEN CLUSTER IONS

Promotor:
Prof.Dr. J. Reuss

EXPERIMENTAL INVESTIGATIONS OF HYDROGEN CLUSTER IONS

PROEFSCHRIFT

TER VERKRIJGING VAN DE GRAAD VAN DOCTOR IN DE WISKUNDE EN NATUURWETENSCHAPPEN AAN DE KATHOLIEKE UNIVERSITEIT TE NIJMEGEN, OP GEZAG VAN DE RECTOR MAGNIFICUS PROF.DR. A.J.H. VENDRIK, VOLGENS BESLUIT VAN HET COLLEGE VAN DECANEN IN HET OPENBAAR TE VERDEDIGEN OP DONDERDAG 2 NOVEMBER 1978 DES NAMIDDAGS TE 4.00 UUR

DOOR

HUBERT ARNOLD VAN LUMIG

GEBOREN TE KONINGSBOSCH

1978

DRUK· STICHTING STUDENTENPERS NIJMEGEN

Bij deze betuig ik mijn dank aan allen die op enigerlei wijze een bijdrage hebben geleverd tot het slagen van het onderzoek en aan het tot stand komen van dit proefschrift. Enkelen wil ik in het bijzonder vermelden.

Dr. A.P.J. van Deursen, die mij heeft ingewijd in de bundeltechniek.

De Heren L. Hendriks, J.J. Holtkamp, E.G.H. van Leeuwen, F.A. van Rijn en C.A. Sikkens voor hun bijdrage tot het oplossen van moeilijkheden op technisch en electronisch gebied.

De Heren C. Verhagen en G. Heusschen, die gedurende hun afstudeerperiode aan dit onderzoek hebben meegwerkt.

Mej. L.H. van Doorn voor al het typewerk.

Alle leden van de groep Atoom- en Molecuulfysica van de Katholieke Universiteit voor hun prettige samenwerking.

I would like to express my deepest gratitude to Dr. A. Ding for his excellent guidance during my stay at the Hahn-Meitner-Institut at W-Berlin.

De technische afdelingen wil ik bedanken in de personen van de Heren J. Gerritsen, J.C.M. van Langen, H. Verschoor en P.C. Walraven.

Aan mijn ouders

Aan Mariet

C O N T E N T S

1.1. Introduction

Investigating the intensity of supersonic molecular beams of hydrogen gas, Becker and co-workers found that condensation of the hydrogen gas occured if the stagnation condition was near to the condensation point (ref. 1). The condensation manifested itself by a dramatic increase of the particle flux in the beam (by a factor of 30) if the pressure in front of the nozzle changed from 62 torr to 97 torr at a source temperature T = 20 K. Further evidence came from time of flight measurements, showing an increase of the average beam velocity due to conversion of the condensation heat into translational energy (ref. 1). The beam flux was monitored by an ionization gauge.

Whether cluster ions could be formed from these molecular clusters by electron bombardment was unknown until 1961. The analysis of the ion signal, obtained by electron bombardment (175 eV) of a condensed CO_2 beam, with a magnetic mass spectrometer put an end to this uncertainty. $(CO_2)_n^+$ cluster ions with $n \leqslant 7$ were observed (ref. 2). The mass spectrum was obtained by sweeping the accelerating voltage between 0.4 and 2.0 keV.

To pursue the investigations of condensation phenomena with an electron bombardment detector, the need of a mass analyser for masses up to 10^5 amu became necessary (ref. 3). A very elegant mass selector has been obtained by the retarding field method (ref. 4). For example, the flow kinetic energy of a $(CO_2)_{1000}$ molecule from a room temperature nozzle expansion can amount to 95 eV. The cluster molecules are ionized by an intersecting electron beam. Thereafter the cluster ions pass through a retarding field electrode system to the ion collector, provided their initial kinetic energy is high enough to overcome the retarding field. By measuring the ion current as a function of the retarding voltage, the mass distribution function of the cluster ions is obtained.

To investigate whether a cluster ion is singly or multiply charged, the time of flight method was employed; accelerating a cluster ion to a given energy, the final velocity depends on the cluster ion charge, as well as its mass. Measuring the flight time of bursts of N_2 cluster ions, accelerated to 10 keV, stable cluster ions of about 22000 nitrogen molecules carrying up to five positive charges have been detected (ref. 5).

Another technique to obtain cluster ions is reported by Clampitt and co-workers (ref. 6). Hydrogen gas is condensed on a copper surface at 3 K. A focused electron beam of 23 eV is swept over this surface. The ions emitted from the target are focused into a quadrupole mass filter. At the onset of condensation H^+ and H_3^+ are observed. As condensation proceeds ion clusters were observed up to m/e = 99. The variety of ion clusters that can be investigated experimentally by this technique seems to be unlimited (ref. 7, 8).

The oldest experimental evidence of ion clustering was given in 1939 by Munson et al. (ref. 9) and was deduced from mobility measurements of alkali metal ions in the rare gases. Also water vapour was shown to cluster to the extent of six neutral molecules binding to each ion. Gas phase equilibria measurements are a refinement of this experiment (ref. 9). Briefly, this technique consists of extracting ions from a thermionic source and transporting them to a field free reaction zone, where clustering reactions proceed to equilibrium under the conditions of a given experiment. The equilibrium ionic species, which drift out of the reaction cell into vacuum through a leak orifice are mass analyzed. By measuring the equilibrium constants as a function of cell temperature for each reaction associated thermodynamic properties are evaluated. The enthalpies for the successive addition of molecules may be taken as a measure of the individual bond energies (ref. 10-14).

An experiment, exploiting the features of both a nozzle expansion and an equilibrium experiment is reported by Fenn et al. (ref. 15). A mixture of H_2O molecules and H^+ ions is expanded through a nozzle. By changing the pressure, temperature and composition of the source gas as well as the diameter of the orifice, the degree and duration of supersaturation to which the ions are exposed can be controlled over a wide range of conditions. The change in the cluster ion distribution during the expansion process provides information on the kinetics of cluster growth. Cluster ions containing up to 20 H_2O molecules could be investigated.

Theoretical calculations about cluster ions are scarce and are limited in general to binding energies and binding distances for small cluster ions (ref. 16-19). A more extensive calculation concerning Ar_nK^+ ($n \leq 12$) ionic clusters has been performed by Etters et al. (ref. 20). A self-consistent field formalism was developed that dynamically determined the thermodynamic properties of these clusters. It is found that at low temperatures, the clusters form crystallites. With increasing temperature the argon atoms are less firmly fixed to their equilibrium position, melting occurs and finally they dissociate spontaneously. The crystallite structures formed by the systems involving 6 and 12 argon atoms were calculated to be octahedral and icosahedral, respectively, with the ion in the middle; they possess a relatively large binding energy.

Two applications of cluster ions of practical importance must be mentioned here. To grow crystalline layers, energy must be supplied to rearrange the atoms arriving at the growing interface, into the crystalline structure. Normally this is achieved by heating the substrate. However, if the material is transported in the form of ionized particles this energy can be supplied directly via acceleration of the ions. Thus, use of ion beams provides the unique possibility of giving the impinging particles well defined kine-

tic energies, greatly exceeding thermal energies.

A limitation to this technique is set by beam space charge effects, limiting both the experimentally accessible energy range to $\geqslant$ 20 eV and the maximum growth rate to roughly 500 Å/min.

By the use of cluster ion beams both limitations are considerably relaxed. Higher growth rates, up to several μ/min, are feasible by using beams of singly charged clusters. The energy, supplied by the accelerating field, is now spread over all the atoms composing a cluster. This feature opens the energy range of 1 to 20 eV/atom, without loss of intensity. Promising results for a Pb cluster ion beam have been obtained (ref. 21-24), and work on a Ag beam is in progress (ref. 25).

Intense beams of hydrogen clusters up to 40 A neutral equivalent (1 A equivalent = 6.10^{18} atoms/s) under pulsed conditions and 150 mA neutral equivalent continuously working have been obtained (ref. 26). These intensities are of interest for the filling of magnetic traps in fusion experiments. For the heating of the plasma neutral hydrogen atoms or molecules can be injected, possessing energies higher than 100 keV. The decisive step to obtain these fast neutrals is the charge transfer of H^+ ions in a Cs-cell to form H-atoms. The efficiency of this process decreases sharply with increasing energy. The energy per atom should preferably be below 100 eV. For this reason, the use of hydrogen cluster ions as primary ions looks very promising. A large positive hydrogen cluster ion can be accelerated to energies corresponding to 100 eV/H_2 molecule. If these cluster ions pass through a Cs cell, large fragmentation and charge exchange occur simultaneously so that strong H_2^- currents may be obtained. Next, these negative ions are accelerated to above 100 keV and neutralized in a Cs-cell (this charge exchange process remains effective up to high energies) before they enter the fusion trap. Work along this line is in progress.

References

1. E.W. Becker, K. Bier und W. Henkes, Z.Phys. 146 (1956) 333
2. W. Henkes, Z.Naturforsch. 16a (1961) 842
3. W. Henkes, Z.Naturforsch. 17a (1962) 786
4. J. Bauchert und O.F. Hagena, Z.Naturforsch. 20a (1965) 1135
5. W. Henkes and G.Isenberg, Int.J.Mass Spectrom.Ion Phys. 5 (1970) 249
6. R. Clampitt and L. Gowland, Nature 223 (1969) 815
7. R. Clampitt and D.K. Jefferies, Nature 226 (1970) 141
8. G.R. Floyd and R.H. Prince, Nature 240 (1972) 11
9. R.J. Munson, K. Moselitz and A.M. Tyndall, Proc.Roy.Soc. 172 (1939) 28 and 43
10. I.N. Tang and A.W. Castleman, Jr., J.Chem.Phys. 57 (1972) 3638
11. I.N. Tang and A.W. Castleman, Jr., J.Chem.Phys. 60 (1974) 3981
12. D.C. Conway and J.H. Yang, J.Chem.Phys. 43 (1965) 2900
13. K. Hiraoka and P. Kebarle, J.Chem.Phys. 62 (1975) 2267
14. R. Kebarle, J.Am.Chem.Soc. 89 (1967) 6393
15. J.Q. Searcy and J.B. Fenn, J.Chem.Phys. 61 (1974) 5282
16. J. Easterfield and J.W. Linnett, Nature 226 (1970) 142
17. M.B. Milleur, R.L. Matcha and E.F. Hayes, J.Chem.Phys. 60 (1974) 2
18. S.W. Harrison, L.J. Massa and P. Solomon, J.Chem.Phys. 62 (1975) 2267
19. R. Ahlrichs, Theor.Chim.Acta 39 (1975) 149
20. R.D. Etters, R. Danilowitz and J. Dugan, J.Chem.Phys. 67 (1970) 1570
21. T. Takagi, I. Yamada and A. Sasaki, Proc. of the 2nd International Conf. on Ion Sources, p. 790, Vienna, September 1972
22. T. Takagi, I. Yamada and A. Sasaki, Proc. of the 6th International Vacuum Congress, Kyoto, March 1974
23. T. Takagi, I. Yamada and A. Sasaki, Proc. of the 2nd Symposium on Ion Sources and Formation of Ion beams, VII-4, Lawrence Livermore

Laboratory, U.S.A., October 1974

24. T. Takagi, I. Yamada and A. Sasaki, Proc. of the International Conference on Ion Implantation in Semiconductors and Other Materials, Osaka, Japan, August 1974

25. A.E.T. Kuiper, private communication

26. B.J.C. Burrows, P.G. Dawson, G.A.G. Motson, E.S. Tay and H.H.H. Watson, Experiments on hydrogen clusters, 5th Symposium on Fusion Technology, Oxford 1968

27. E.W. Becker, H.D. Falter, O.F. Hagena, W. Henkes, R. Klingelhöfer, H.O. Moser, W. Obert and I. Poth, Nucl.Fusion 17 (1977) 617

1.2. The present investigations

In the present experiment the production of hydrogen cluster ions is performed by supersonic expansion of a cooled hydrogen gas followed by electron bombardment of the cluster molecules. Unlike the experiments discussed in the introduction, it was not our primary interest to investigate condensation and ionization phenomena. Our goal was to obtain information about the structure and stability of small hydrogen cluster ions.

In chapter two results are presented for attenuation measurements of hydrogen cluster ions colliding with nitrogen. The measurements were performed both with and without second mass analysis. The energy range investigated runs from 250 up to 890 eV. The mass range extends from H_2^+ up to H_{27}^+.

The total collision cross sections showed a slight screening between the H_2 molecules (nonlinearity in the number N of H_2 molecules) interpreted with an opacity model for the cluster ions. This model yielded a value for the density n_2 of the H_2 molecules in the cluster ion. Repetition of the same measurements at a later stage of the experiment with higher accuracy did no longer show a clear screening effect. The value $n_2 = 0.025\ \text{Å}^{-3}$ is thus an upper limit for the H_2 density in the cluster ions.

The energy dependence of the total collision cross section for the cluster ions is interpreted in terms of a potential model.

The difference between the attenuations measured with and without second mass analysis is explained in terms of fragmentation of colliding cluster ions. Fragment ions which are scattered in forward direction are detected if no mass analysis is applied; with mass analysis they are rejected. The intensity of the primary cluster beam was too low to observe the fragment ions independently.

Chapter three deals with attenuation and fragmentation measurements of hydrogen cluster ion beams with He as scattering partner. The intensity of the beam is improved by a factor 10^4 relative to the intensities available earlier.

Results are presented for the total collision cross section of hydrogen cluster ions H^+_{2n+1}; $n \leq 20$ in the energy range from 200 to 850 eV. It will be shown that the cross section increases linearly with the number of H_2 molecules of the cluster ion; no screening is observed. We also interprete the energy dependence of the total collision cross sections in terms of potential scattering; again, reasonable values for s are obtained, although the observed fragmentation renders the use of a simple potential model questionable.

With the higher intensity of the primary beam, the fragment intensities were readily measured. It turns out that fragmentation occurs to all fragment ions smaller than the parent ion. By measuring fragment intensities as function of the density in the scattering chamber, relative values for the fragmentation cross section are determined. The results are obtained with a fixed acceptance angle of the detector of 10^{-4} sterad.

Furthermore, the fragmentation cross sections as function of the fragment mass show peaks at the position of certain fragment masses. Apparently these fragment ions, H^+_9, H^+_{15}, H^+_{19}, H^+_{23}, H^+_{27}, are particularly stable.

Chapter four presents results for the differential fragmentation cross sections for parent ions H^+_5 up to H^+_{15} and most of their fragment ions with argon and hydrogen as scatter gas. The energy ranges from $\bar{E}_0 = 6.8$ up to $E_0 = 75$ eV.

The differential fragmentation cross sections reduce to unique curves for each fragmentation process by plotting them against $\theta\sqrt{E_0/E_{ref}}$. This result tells us that the fragmentation process is independent of the incoming

parent ion energy, if viewed by an observer travelling with the parent ion velocity.

A model, containing a single parameter, the unique energy of each evaporated H_2 molecule, is able to describe both the angle as well as the velocity dependence of the differential fragmentation cross section for all parent and fragment masses.

From the differential measurements we learn that the finite acceptance angle of the measurements described in chapter three plays an important role for the relative values for the fragmentation cross sections. The corrected results become rather independent of the fragment and parent mass; a result, also obtained directly from the differential measurements. The preferential fragmentation to relatively stable fragment ions again is observed.

International Journal of Mass Spectrometry and Ion Physics, 25 (1977) 137—145 137

COLLISIONS OF HYDROGEN CLUSTER IONS WITH A GAS TARGET AT 250—900 eV ENERGY *

A. VAN LUMIG and J. REUSS

Fysisch Laboratorium, Katholieke Universiteit, Toernooiveld, Nijmegen (The Netherlands)

(First received 2 February 1977; in final form 23 March 1977)

ABSTRACT

Results of attenuation measurements of hydrogen cluster ion beams with N_2 as scattering partner are presented. The mass of the cluster ion is varied from H_2^+ to H_{17}^+. Except for H_2^+, only the odd masses had sufficient intensity to be detected. The measured H_2^+ ion current amounts to 10^{-13} A at an ion energy of 890 eV. For the smallest odd cluster ions, e.g. H_5^+, the ion current is a factor of 100 lower and decreases slowly with increasing size of the ion.

The measurements have been performed at three laboratory ion energies, 250, 510 and 890 eV, with and without mass analysis of the attenuated beam. The attenuation of the H_2^+ signal is always substantially larger than the attenuation of the H_3^+ signal, confirming a larger bonding distance at H_2^+ compared to H_3^+ [1].

A model for the cluster ions is suggested as a result of the measurements obtained with mass analysis of the attenuated beam. The parameter of this model is the density n_2 of H_2 molecules in the cluster ion, which is found to be $n_2 = (0.025 \pm 0.005)$ Å^{-3}. Comparing this value with $n = 0.02$ Å^{-3}, which is valid for the density of H_2 molecules in liquid hydrogen, a small contraction of the cluster ion, due to the charge in its centre, is found. Assuming the cluster ion to be scattered by a potential of the form $V(r) = -C_s/r^s$, s rises from $s = 4$ for H_3^+ to $s = 11$ for cluster ions larger than H_9^+. Thus the "soft" H_3^+ core is increasingly screened by H_2 molecules.

Differences between measured attenuations with and without mass analysis of the attenuated beam are caused by the fragmentation of cluster ions upon collision. These fragments are mainly scattered in the forward direction and are detected if no mass analysis of the attenuated beam is applied. It is demonstrated that whether or not a cluster ion disintegrates into fragments upon collision depends sensitively on its laboratory energy and its mass. This behaviour can be understood in terms of a shell model.

INTRODUCTION

Amongst other purposes the aim of our experiment is to obtain information concerning the structure, stability and total collision cross-section of

* This work is part of the research program of the "Stichting voor Fundamenteel Onderzoek der Materie (F.O.M.)" and has been made possible by financial support from the "Nederlandse Organisatie voor Zuiver Wetenschappelijk Onderzoek (Z.W.O.)".

cluster ions. Theoretical information is scarce and limited to the smallest cluster ions [1—4].

In our apparatus the formation of cluster ions occurs by ionization of a neutral cluster beam from a nozzle source [5]. Ionization is effected by an electron bombardment ionizer (electron energy ca. 100 eV).

Other measurements on cluster ions were done with a pulsed electron beam high pressure ion-source mass spectrometer [6] and with the drift-tube mass spectrometer [7]. In the first case a gass at a pressure of ca. 1 torr is ionized, giving rise to cluster ions from ion reactions in the ionizer; in the second case an ion beam drifting through a gas undergoes attachment processes from the gas molecules. In contrast to our technique, however, both approaches produce only small signals of heavy cluster ions.

The analysis of the attenuation results is performed using a classical interpretation. For such an interpretation to be appropriate, the scattering process has to meet two conditions. The trajectory of the particle must be well defined (which requires that its wavelength, k^{-1}, is small compared to the radius of the interaction potentials, a). Furthermore, the deflection angle θ during the collision must be well defined (which requires that the momentum transfer $\hbar k$ is large, $k >> 1/a$). Both conditions are satisfied if [8]

$$\theta \gg \hbar/\mu g a$$

Here μ stands for the reduced mass of the collision partners and g for the relative velocity.

In the case of H_2^+, for an ion energy of 250 eV and an interaction radius of 3 Å, $\hbar/\mu g a \approx 6 \times 10^{-4}$ rad. The detection angle of our apparatus was $\theta \approx 10^{-2}$ rad. Thus, classical theory can be applied to our results.

Classical small angle scattering

Consider the scattering problem for particles with energy, E_r, and with a potential of the form $V(r) = -C_s/r^s$. The deflection angle, θ, is a function of the impact parameter, b. If θ is small enough we can use the two approximations that the momentum, P_z, along the path remains unchanged and that the perpendicular forces, F_x, cause a transverse momentum, P_x, which can be calculated as if the encounter would take place along straight trajectories

$$P_x = \int_{-\infty}^{\infty} F_x \, dt = \frac{1}{g} \int_{-\infty}^{\infty} F_x \, dz$$

For small angles, $\theta = P_x/P_z$ yields

$$\theta = -\frac{d}{db} \frac{1}{\mu g^2} \int_{-\infty}^{\infty} V(r) \, dz$$

Substituting $V(r) = -C_s/r^s$ and $u = z/b$ one finds [9]

$$\theta = -\frac{C_s}{\frac{1}{2}\mu g^2 b^s}\left[\frac{s}{2}\int_{-\infty}^{\infty}\frac{\mathrm{d}u}{(1+u^2)^{(s+2)/2}}\right]$$

Substituting $K_s = -C_s[\frac{s}{2}\int_{-\infty}^{\infty}(\mathrm{d}u)/(1+u^2)^{(s+2)/2}]$ which depends only on the strength of the potential and the power used in the potential, and $E_r = \frac{1}{2}\mu g^2$, a simple relation results between θ, E_r and b

$$\theta = \frac{K_s}{E_r b^s} \tag{1}$$

The effective collision cross section σ_{int} can be written as

$$\sigma_{int} = 2\pi\int_0^{b_{max}} b\,\mathrm{d}b = \pi b_{max}^2 \tag{2}$$

where b_{max} is the largest impact parameter, which can lead to a deflection larger than the detection angle, $\theta_{min} = K_s/E_r b_{max}^s$. Setting the lower limit of the integral over b equal to zero means that all particles with impact parameters less than b_{max} miss the detector. (If, however, the beam particles are heavier than the scatterer, nearly head-on collisions may cause both particles to be accepted by the detector, after the collision. In all our measurements the scattering partner was heavier than the beam particle, so that the lower limit in eqn. (2) can be set at zero.)

From the last two equations

$$\sigma_{int} = \frac{K_s'}{(E_r\theta_{min})^{2/s}} \tag{3}$$

with $K_s' = \pi \cdot K_s^{2/s}$.

This equation can be expressed in terms of quantities occurring in the laboratory system if E_r is expressed in terms of the beam laboratory energy, E, and the relative angle, θ_{min}, is expressed in terms of the laboratory detection angle, θ_d. If θ_{min} and θ_d are both small, $\theta_{min} = ((m_1 + m_2)/m_2) \cdot \theta_d$ [9], and if the initial velocity of the target particle is negligible compared to that of the beam particle, $E_r = (m_2/(m_1 + m_2)) \cdot E$. Thus, $E_r\theta_{min} = E\theta_d$ and eqn. (3) expressed in laboratory coordinates remains formally unchanged.

$$\sigma_{int} = \frac{K_s'}{(E\theta_d)^{2/s}} \tag{4}$$

Assuming that all cluster ions are scattered by the same type of potential, V_s, differences in cross-sections between the cluster ions must be attributed to different values of K_s'.

Apparatus

In Fig. 1, the apparatus is sketched. During operation the 25-μm diameter nozzle source, S, is kept at a temperature of 30 K; the source pressure is varied between 200 and 1000 torr.

Cluster ions are produced in an electron bombardment ionizer, I, (electron energy 100 eV). The cluster ions are accelerated and mass selected by mass spectrometer, MS_1. Having passed through a scattering chamber, SC, the beam can be detected with and without mass analysis by a second magnet, MS_2.

To prevent disturbing oil films on the inside of the vacuum envelope a number of precautions have been taken. All walls in the part of the apparatus behind the ionizer are baked continuously at 100°C by hot foils; walls near to the ion beam are gold-plated. The scattering chamber, which during operation is cooled down to liquid nitrogen temperature, is equipped with a heating element. Between measurements it is kept at 250°C.

The beam is collimated by means of a slit, CS, of variable width 50 cm upstream of the scattering chamber, SC, the scattering entrance slit (0.8 × 10 mm^2), and two detector slits. The first of these, DS_1, is positioned in front of the mass analyser MS_2 50 cm downstream from the scattering chamber with four possible widths (0.2, 1.5, 2.0 and 4.0 mm), the second DS_2, at

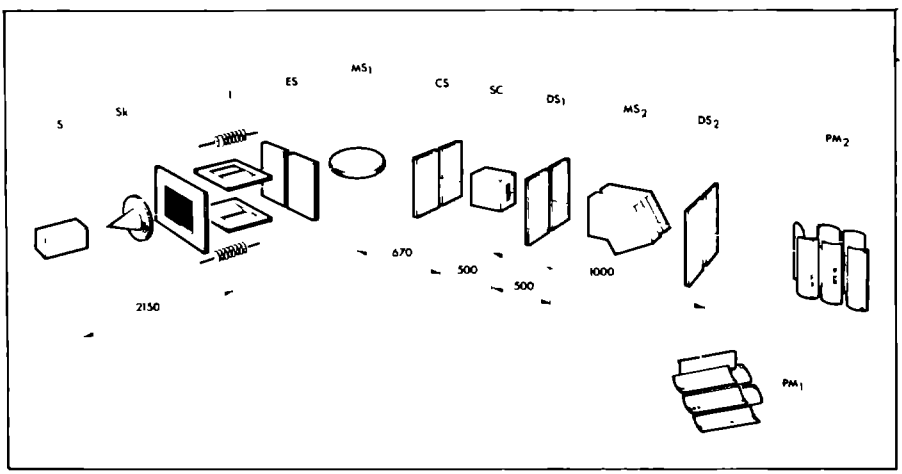

Fig. 1. The apparatus. The cluster beam is formed by the nozzle source S and the skimmer Sk. After the ionizer I, the ion beam passes through the entrance slit ES into the first mass spectrometer MS_1. The mass selected beam is focused on the collimation slit, CS, passes through the scattering chamber SC and is detected in two ways: either the beam follows a straight trajectory through the detector slit DS_2 into the particle multiplier PM_2 or it is mass analysed in MS_2, collimated by DS_1 and finishes in PM_1.

100 cm from the scattering center is for collimation if no mass analysis is applied — this latter slit is continuously variable.

RESULTS AND DISCUSSION OF THE MEASUREMENTS WITH MASS ANALYSIS OF THE ATTENUATED BEAM

In Fig. 2 results of the scattering of hydrogen cluster ions against N_2 are presented. The measurements were performed at three energies, 250, 510 and 890 eV. Results are presented for the mass range H_2^+—H_{21}^+.

On the horizontal axis the masses of the cluster ions are given and on the vertical axis the values of $-\ln(I_{an}/I_0)$ where I_{an} stands for the attenuated and I_0 for the unattenuated intensity with mass analysis.

The beam was collimated by CS (0.8 × 13 mm²), the entrance slit of the scattering chamber (0.8 × 10 mm²) and the detector opening (4 × 17 mm²).

The large attenuation of H_2^+ compared to the attenuation of H_3^+ is striking. Two reasons can be used to explain this effect. First, the bonding distance in

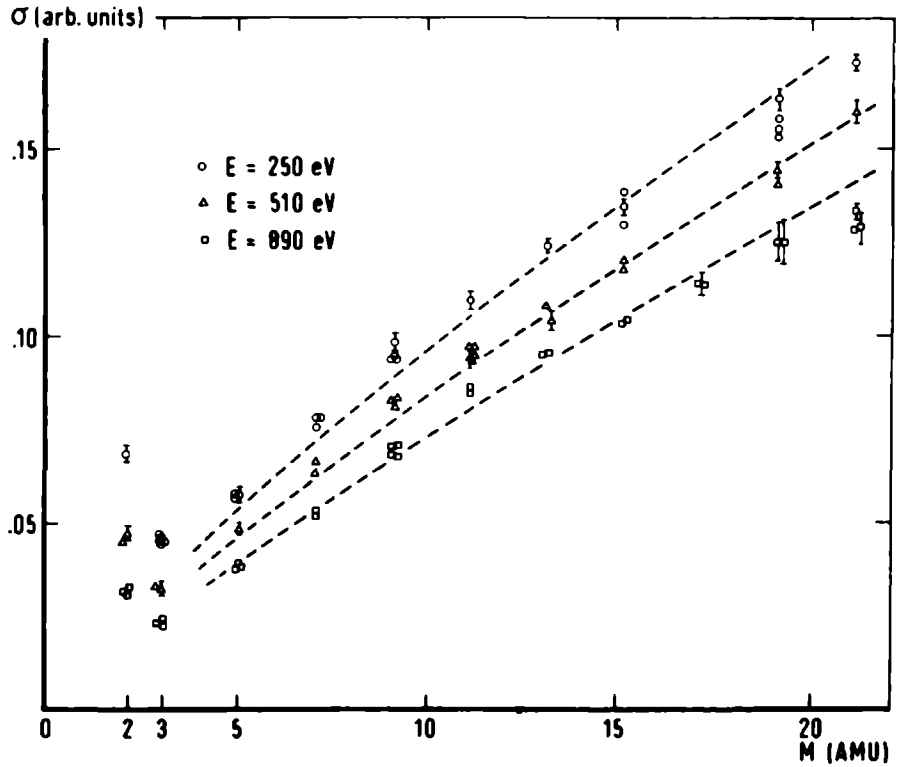

Fig. 2. Apparent cross-sections, obtained with mass analysis of the attenuated beam, vs. cluster masses for the three laboratory energies. The dashed lines correspond to eqn. (9).

H_2^+ is about a factor of 1.2 larger than the bonding distance in H_3^+ [1]. Second, the H_2^+ ion is probably in a high vibrational state, whereas the H_3^+ ion can cool down during the formation, by transferring part of its internal energy to the H atom leaving the ionized cluster molecule $(H_2)_2^+$.

The values of $-\ln(I_0/I_{an})$ are proportional to σ_{int} and show a linear behaviour as a function of the mass for the lower masses (see Fig. 2). In our interpretation the H_2 molecules in the cluster ion add about equally to the cross-section, for small cluster ions. Defining N as the number of H_2 molecules in the cluster ion, σ_2 as the increment of σ_{int} if an H_2 molecule is added to a small cluster ion and σ_3 as the integral cross-section of H_3^+ we find

$$\sigma_{int}(N) = N\sigma_2 + \sigma_3 \tag{5}$$

This type of linear dependence is observed up to mass H_{13}^+, at an ion energy of 890 eV. Above this linear region a screening effect occurs. A uniform density n_2 of H_2 molecules is assumed for all cluster ions, and the cluster ion is supposed to form a sphere. With N as the number of H_2 molecules in the cluster ion its radius R is given by

$$R = \left(\frac{3}{4\pi}\,\frac{N}{n_2}\right)^{1/3} \tag{6}$$

This model does not adequately account for the H_3^+ central ion. The way H_3^+ is actually taken care of is to assume that it resembles 1.5 H_2 molecule. As a consequence results for the lower mass are less accurate; the cross-sections calculated are too high. For the larger cluster masses this error is negligible.

Defining an opacity function $\xi(b)$ for a cluster ion

$$\xi(b) = 1 - e^{-n_2 l \sigma_2} \tag{7}$$

with $l = 2\sqrt{R^2 - b^2}$, σ_N becomes

$$\sigma_N = 2\pi \int_0^R \xi(b) b\, db = 2\pi \int_0^R (1 - e^{-n_2 l \sigma_2}) b\, db \tag{8}$$

Evaluation of eqn. (8) yields

$$\sigma_N = \pi R^2 + \frac{\pi}{2}\,\frac{2R}{\sigma_2 n_2} \cdot e^{-2R\sigma_2 n_2} + (e^{-2R\sigma_2 n_2} - 1)\frac{\pi}{2}\,\frac{1}{\sigma_2^2 n_2^2} \tag{9}$$

In eqn. (9) the only free parameter is n_2. Substituting values for σ_2, obtained from the experiment, and fitting the measurements to eqn. (9) a value of 0.025 ± 0.005 Å^{-3} has been found for n_2. Comparing this value with $n = 0.02$ Å^{-3}, which describes the density of H_2 molecules in the liquid state, a small contraction of the cluster ion is found, due to the charge in its centre. In Fig. 2 this fit is represented by the dashed lines.

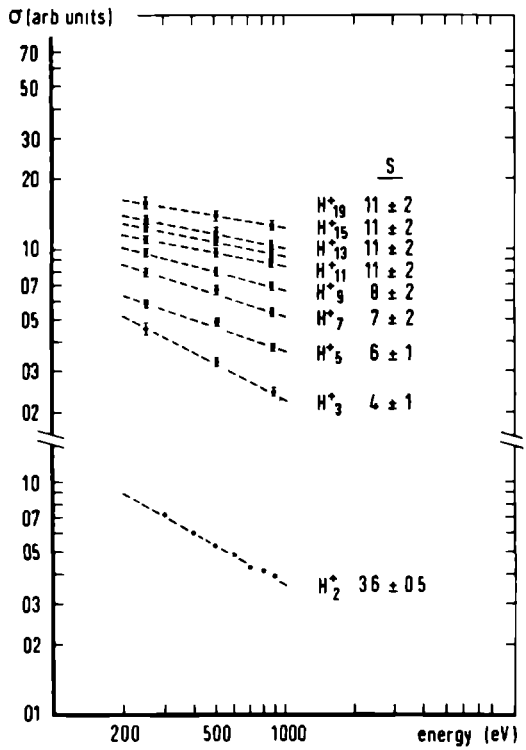

Fig. 3. Apparent cross-sections, obtained with mass analysis of the attenuated beam, vs. laboratory energy. The value of s corresponds to the exponent in eqn. (4).

Energy dependence of the cross-section of cluster ions

In Fig. 3 a log—log plot is shown for the cross-sections of a number of cluster ions as functions of the laboratory energy. On the horizontal axis the laboratory energy is plotted and on the vertical axis σ_{int}.

From eqn. (4) the slope of the straight lines in Fig. 3 gives the value of s. It is found that s varies from $s = 4 \pm 1$ for H_2^+ up to $s = 11 \pm 2$ for cluster ions larger than H_9^+. Apparently the "soft" H_3^+ core is increasingly screened by "hard" H_2 molecules, going to larger cluster ions.

COMPARISON OF THE RESULTS OBTAINED BOTH WITH AND WITHOUT MASS ANALYSIS OF THE ATTENUATED BEAM

In Fig. 4 results are presented obtained with and without mass amalysis downstream from the scattering chamber. On the horizontal axis the mass of the cluster ions is plotted and on the vertical axis the respective values of

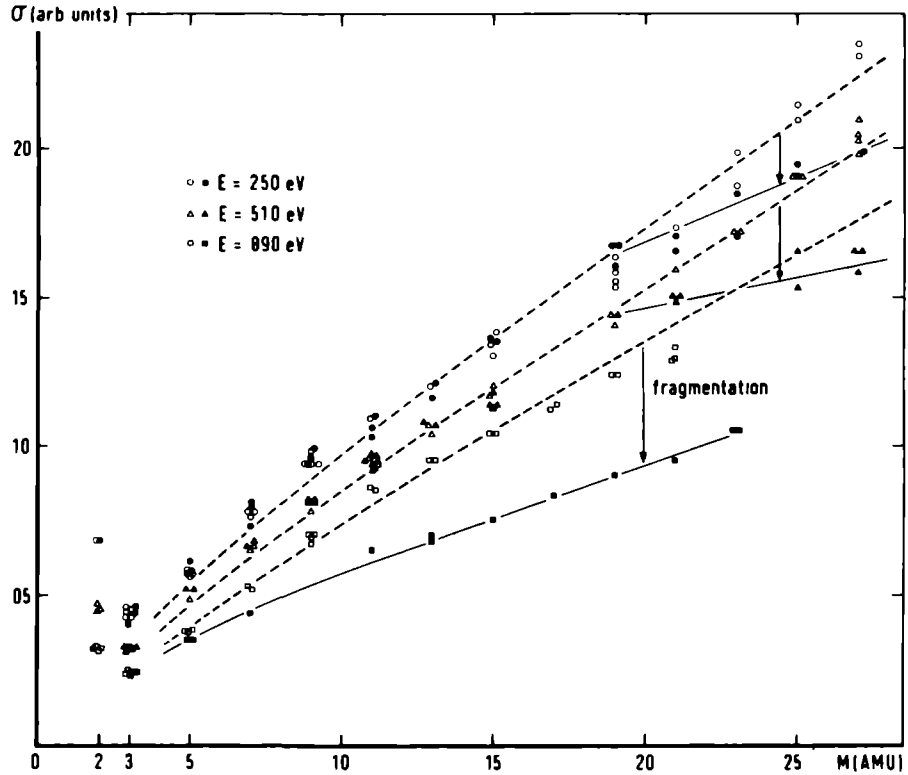

Fig. 4. Apparent cross-sections vs. mass for hydrogen cluster ions, with (open symbols) and without (closed symbols) second mass analysis. The dashed lines correspond to eqn. (9). The full lines indicate the influence of fragmentation.

$-\ln(I_{an}/I_0)$ and $-\ln(I_{nan}/I_0)$; I_{an} and I_{nan} stand for the attenuated intensity with and without second mass analysis, respectively. The collimation of the beam is the same as discussed before.

Let us first consider the mass range below H_{21}^+. It appears that the results obtained at 250 and 510 eV differ from the results obtained at 890 eV. At the highest energy the two curves belonging to $-\ln(I_{an}/I_0)$ and $-\ln(I_{nan}/I_0)$ diverge above H_3^+. This splitting of the two curves at 890 eV is explained in terms of the fragmentation of cluster ions during scattering. The fragments are scattered in the forward direction, and will be detected if no mass analysis of the attenuated beam is applied. Thus, fragmentation starts at H_5^+ as could be expected considering the small binding energy (0.3 eV) of the H_2 molecule to the H_3^+ core [1].

The fact that the two curves at the lowest energies nearly coincide means that fragmentation is less probable. Thus, it is clear that the fragmentation cross-

section is strongly dependent on the energy of the cluster ions. In the case of H_9^+, the energy dependence of the fragmentation cross-section has been investigated more thoroughly. It appeared that fragmentation rapidly increases above 800-eV laboratory energy.

Defining $\Delta\omega = \Delta E/\hbar$, (with ΔE the energy necessary to split off a H_2 molecule from e.g. H_9^+) and $\Delta\tau = l_c/g$ (with l_c the interaction length and g the relative velocity, for instance of H_9^+ and N_2 at 800-eV laboratory energy) the product $\Delta\omega\Delta\tau$ yields $\Delta\omega\Delta\tau \sim 0.7$. This result indicates that the Massey criterium must be considered which appears to impede fragmentation below 800 eV.

Let us now consider the total available mass range. From Fig. 4 it is clear that fragmentation does occur at the two lowest energies for masses larger than H_{19}^+. Applying the Massey criterium to these masses, it is found that the binding energy of these masses must be at least a factor of two lower than the binding energy of H_9^+.

This result is very interesting, because is suggests that the H_2 molecules in a cluster ion are packed in shells. A cluster ion consists of a H_3^+ core, a first shell which may contain about 8 H_2 molecules and a second shell starting with the 9th H_2 molecule with a binding energy at least a factor of two lower than the binding energy of the first shell.

REFERENCES

1 R.E. Christoffersen, J. Chem. Phys., 41 (1964) 960.
2 J.T.J. Huang, M.E. Schwartz and G.V. Pfifer, J. Chem. Phys., 56 (1972) 755.
3 S.W. Harrison, L.J. Massa and P. Solomon, J. Chem. Phys., 62 (1975) 2267.
4 K. Hiraoka and P. Kebarle, Nature London, Phys. Sci., 245 (1973) 31.
5 A.v. Deursen and J. Reuss, Int. J. Mass Spectrom. Ion Phys., 11 (1973) 483.
6 A.J. Cunningham, J.D. Payzant and P. Kebarle, J. Am. Chem. Soc., 94 (1972) 7627.
7 D.L. Albritton, T.M. Miller, D.W. Martin and E.W. McDaniel, Phys. Rev., 171 (1968) 94.
8 E.W. McDaniel, V. Cermák, A. Dalgarno, E.E. Ferguson and L. Friedman, in Ion—Molecule Reactions, Wiley-Interscience, New York, 1970, p. 184.
9 I. Amdur and J.E. Jordan, in J. Ross (Ed.), Molecular Beams, Interscience, New York, 1966, p. 40.

International Journal of Mass Spectrometry and Ion Physics, 27 (1978) 197—208 197

COLLISIONS OF HYDROGEN CLUSTER IONS WITH A GAS TARGET, AT 200—850 eV ENERGY ★

A. VAN LUMIG and J. REUSS

Fysisch Laboratorium, Katholieke Universiteit, Toernooiveld, Nijmegen (The Netherlands)

(First received 3 October 1977; in final form 21 November 1977)

ABSTRACT

Results of attenuation and fragmentation measurements of hydrogen cluster ion beams are presented with He as scattering partner. The mass of the cluster ions is varied from H_2^+ to H_{41}^+. Except for H_2^+, only the odd masses had sufficient intensity to be detected. The ion energy ranges from 200—850 eV. Only results of attenuation measurements obtained with mass analysis of the attenuated beam are presented.

Contrary to the N_2 results [1], it is found that for the H_2^+ signal the attenuation is smaller than for the H_3^+ signal. The attenuations of the cluster ion signals show a linear behaviour as a function of the mass of the ions up to H_{41}^+. Thus, within the experimental accuracy, little screening [1] occurs between the H_2 molecules in the cluster ions. Assuming that the ions are scattered by a potential of the form $V(r) = -C_s/r^s$, s rises from $s = 5$ for H_2^+ and H_3^+ to $s = 7$ for ions larger than H_{17}^+, demonstrating the influence of the H_2 molecules upon the attenuation.

Head-on or nearly head-on collisions between particles in the cluster ion with a helium atom cause fragmentation of the ion. All possible fragment ions larger or equal than H_3^+ occur with a variation in intensity of about a factor 2×10^3 in the mass range investigated. The acceptance angle of our apparatus is ca. 10^{-4} sterad. The velocity of the fragment ions approximately equals the velocity of the original cluster ion. Effects of the binding energy of the H_2 molecules to the cluster ion upon the fragment velocity could not be resolved. It appears that fragmentation towards H_9^+, H_{15}^+ and H_{27}^+ has a larger cross-section than to their respective neighbours. We infer that these cluster ions are particularly stable.

INTRODUCTION

This paper deals with two topics: (1) integral collision cross-section measurements, similar to those described in an earlier paper [1], and (2) fragmentation cross-section measurements.

The existence of particularly stable cluster ions is mentioned in the literature. By sweeping a low-energy (23 eV) electron beam over a condensed H_2 surface, a predominant number of H_{15}^+ ions was formed [2]. By the same

★ This work is part of the research program of the "Stichting voor Fundamenteel Onderzoek der Materie (F.O.M.)" and has been made possible by financial support from the "Nederlandse Organisatie voor Zuiver Wetenschappelijk Onderzoek (Z.W.O.)".

technique the ions $Li^+(H_2)_n$ and $Li^+(Ne)_n$, with $n \leqslant 6$, were preferentially produced [3].

Intensity measurements of hydrogen cluster ion beams, produced by supersonic expansion and electron bombardment, reflect the high stability of H_9^+, H_{15}^+ and H_{27}^+ ions (refs. 4, 5 and this paper). The results of a determination from gas phase equilibria of the stabilities of H_5^+, H_7^+, H_9^+ and H_{11}^+ [6] were compatible with theoretical predictions [7].

Recent calculations [8] on the $K^+(Ar)_n$ system showed that $K^+(Ar)_3$, $K^+(Ar)_6$ and $K^+(Ar)_{12}$ are particularly stable.

Using fragmentation cross-section measurements we wish to present further and direct proof of the high stability of H_9^+, H_{15}^+ and H_{27}^+. Furthermore, indications are found that H_{19}^+ and H_{23}^+ are also relatively stable.

The apparatus has been described elsewhere [1]. Relative to the ion intensities reported, an intensity gain of a factor of 10^4 has been achieved by a new ion source set-up. The distance between nozzle hole and ionizer is reduced to 150 mm; new pure tungsten filaments are used in the ionizer, allowing a much higher emission (90 mA); the background pressure in the source chamber is lower than 10^{-4} torr, even at the highest gas load. The collimation of the beam is kept the same: the entrance slit of the scattering chamber [0.8×10 mm^2], and the detector opening [4×13 mm^2] are mounted at distances of 500 and 1000 mm, respectively, from the first collimator slit [0.8×13 mm^2] (see Fig. 1 of ref. 1).

INTENSITY MEASUREMENTS

In Fig. 1 results of intensity measurements of hydrogen cluster ion beams are presented. The source pressures are displayed on the horizontal axis, and on the vertical axis the corresponding intensities of the cluster ions are given on a log-scale. The results of Fig. 1 were obtained using a 15-μm nozzle diameter and a source temperature of 30 K with a nozzle skimmer distance of ca. 10 mm. The ions were accelerated to an energy of 500 eV. Similar measurements were performed elsewhere [4,5]. For the present interest in stable cluster configurations a limited discussion of Fig. 1 suffices. We are concerned with the relative positions of neighbouring curves. In the comparison of these curves, effects due to the transmission of the apparatus or the multiplier efficiency will have little influence.

Note that the parent signal of H_9^+ is formed at higher pressures than the parent signal for ions of smaller masses. The maximum intensity of the H_9^+ signal is however larger than the maximum signal of H_7^+. A similar observation holds for H_{15}^+. The maximum signal of H_{27}^+ is only slightly smaller than the maximum signal of H_{25}^+. These features indicate already that the cluster ions H_9^+, H_{15}^+ and H_{27}^+ are particularly stable.

Another group of cluster ions which would probably be interesting to investigate starts at H_{31}^+. The facts that the intensities of H_{33}^+ to H_{39}^+ rise above the intensity of H_{31}^+, and that the height of the maximum of H_{35}^+ exceeds that

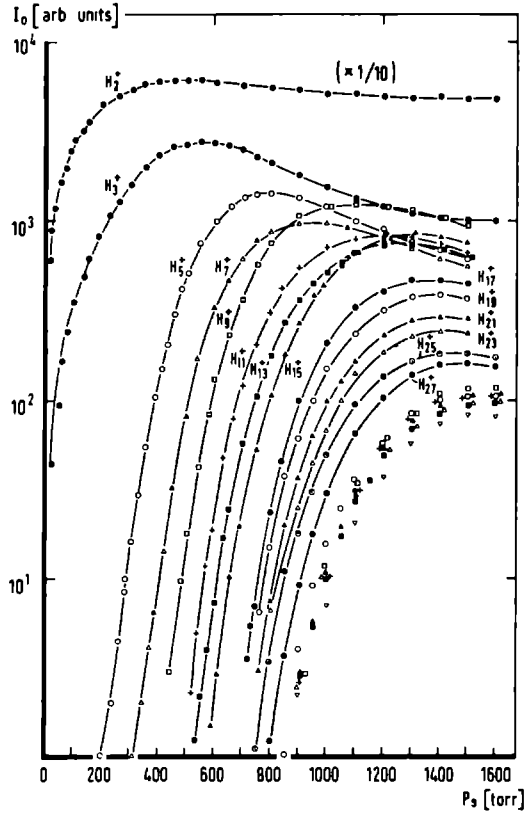

Fig. 1. Intensity I_0 versus source pressure P_s. Results for the heavy ions H_{29}^+ (○), H_{31}^+ (■), H_{33}^+ (▲), H_{35}^+ (□), H_{37}^+ (+), H_{39}^+ (△) and H_{41}^+ (▽) nearly coincide.

of H_{33}^+ and H_{37}^+ (indicating that H_{35}^+ is particularly stable) point to interesting configurations. However, fragmentation measurements for these masses fall outside the present possibilities.

INTEGRAL COLLISION CROSS-SECTIONS

Results of the scattering of hydrogen cluster ions against He are shown in Fig. 2. The measurements have been performed with mass analysis of the attenuated beam. Results are shown for 200, 500 and 850 eV over the mass range H_2^+—H_{41}^+.

The masses of the cluster ions are given on the horizontal axis and on the vertical axis the values of $-1/P \ \ln(I_{an}/I_0)$, where I_{an} stands for the attenuated, I_0 for the unattenuated intensity and P for the pressure in the scattering chamber. This expression is proportional to the integral cross-sec-

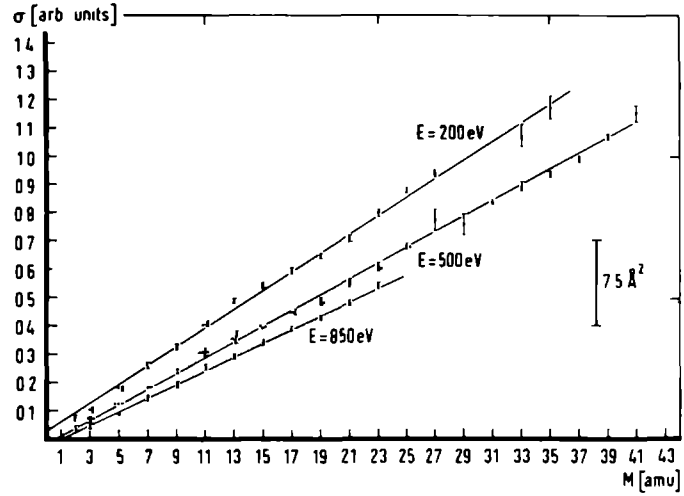

Fig. 2. Integral cross-section σ versus ion mass M. Within 30%, the absolute value can be found from the 7.5-$Å^2$ bar. All measurements can be represented by straight lines, for a fixed energy.

tion σ_{int}. To obtain absolute values, the length l (5 cm) of and the pressure P (calibration factor $P_{He}/P_{N_2} = 6$) in the scattering chamber, as well as the experimental attenuation were used. This absolute value is estimated to be accurate within ±30%.

Contrary to the N_2 results [1], with He as scattering partner less attenuation is found for the H_2^+ signal than for the H_3^+ signal . The binding distance and the vibrational state of the H_2^+ and H_3^+ ions are better probed by He than by N_2. Thus the explanation given in ref. 1 for the N_2 results is insufficient. (At this moment, we can give no explanation for the minimum of the integral cross-section at mass-3, an observation with N_2 as scattering partner. In the mean time this observation was confirmed by us by new measurements with N_2 and a variety of other scattering partners: Ar, SF_6, CO_2, O_2. Only for He and Ne was this minimum absent.)

The values of $-1/P \ln(I_{an}/I_0)$ show a linear dependence on the mass up to mass H_{41}^+. According to the model for the cluster ions, presented in an earlier paper [1], this means that little screening occurs between the H_2 molecules in the cluster ions, in agreement with the small increment of σ_{int} if an H_2 molecule is added to a small cluster ion. The values for the increment which are used in the model are 2.3, 1.9, 1.6 $Å^2$ ± 0.2 $Å^2$, respectively at 200-, 500- and 850-eV ion energy, which are a factor of 1.4 smaller than the values found in the N_2 measurements.

ENERGY DEPENDENCE OF THE CROSS-SECTIONS OF CLUSTER IONS

In Fig. 3 a log–log plot is shown for the cross-sections σ_{int} of a number of cluster ions as a function of the laboratory energy. Assuming the cluster ions to be scattered by a potential of the form $V(r) = -C_s/r^s$, σ_{int} can be expressed as a function of the laboratory energy E and the detector angle θ [1]

$$\sigma_{int} = \frac{K_s'}{(E\theta)^{2/s}} \tag{1}$$

with

$$K_s' = \pi \left[C_s \sqrt{\pi} \cdot s \frac{\Gamma((s+1)/2)}{\Gamma((s+2)/2)} \right]^{2/s}$$

One of the conditions for the validity of eqn. (1) is that cluster ions miss the detector at nearly head-on collisions. Since He has a much smaller mass than most of the cluster ions, this condition is not necessarily fulfilled. However, nearly head-on collisions result in fragmentation of the ion with high probability. The fragment misses the detector because of the second mass analysis. Thus, in the case of helium as scattering partner, this condition has also been met.

Using eqn. (1) the slope of the straight lines in Fig. 3 gives the value of s. It is found that s varies from $s = 5$ for H_2^+ and H_3^+ to $s = 7$ for cluster ions larger

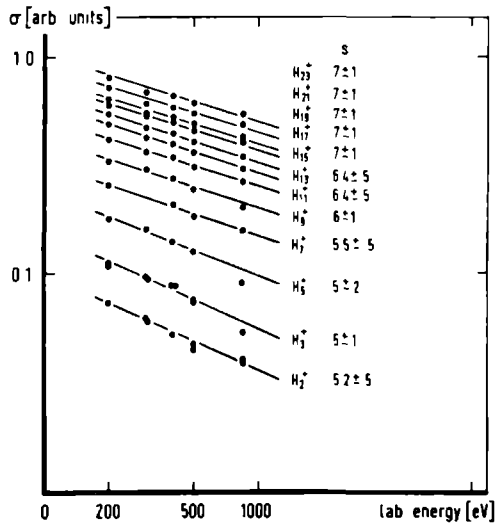

Fig. 3. The energy dependence of the integral cross-sections. The drawn lines correspond with an r^{-s}-dependence of the potential.

than H_{17}^+; for comparison, for collisions with N_2, we found $s = 4$ for H_2^+ and H_3^+ and $s = 11$ for cluster ions larger than H_{11}^+ [1].

According to the results of Mittman et al. [9] one has $E \cdot \theta_{\text{rainbow}} \simeq 110 \cdot \epsilon$. Here, ϵ stands for the depth of the potential minimum and θ_{rainbow} is measured in degrees. We further conclude that $\epsilon(H_{2n+1}^+ - He) \lesssim 0.6$ eV because of the fact (a) that H_2^+, H_3^+, H_5^+, ... represent progressively more shielded Coulomb charges, (b) that $\epsilon(H^+ - He) \simeq \frac{1}{2}\epsilon(H^+ - Ar)$ and (c) that $\epsilon(H_2^+ - Ar) \simeq 1.3$ eV. From $\epsilon \simeq 0.6$ eV follows that $\theta_{\text{rainbow,lab}} = 0.3°$ at 200 eV and 0.08° at 800 eV whereas our measurements of the integral cross-section probe collisions with a deflection angle $\theta_{\text{lab}} \gtrsim 0.2°$. Consequently, the migration of the rainbow maximum into the detector slit is probably reflected by the stronger energy dependence of the small clusters.

FRAGMENTATION OF HYDROGEN CLUSTER IONS BY COLLISIONS

As an example, Fig. 4 shows the result of a mass scan with the second magnet, when H_{29}^+ is selected by the first magnet and sent through the scattering chamber which is filled with He to a pressure of ca. 10^{-3} torr. The energy of the beam is 500 eV and the acceptance angle of the apparatus is ca. 10^{-4} sterad.

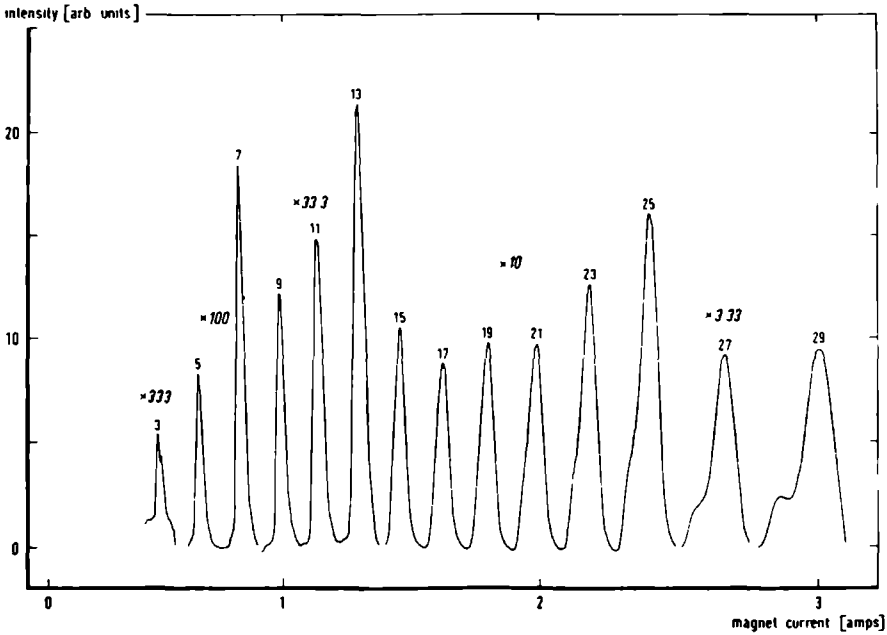

Fig. 4. Fragment peaks, for the H_{29}^+ parent ion at 500-eV collision energy, with He at 10^{-3} torr in the collision chamber. Note the different sensitivities with which the uninterrupted curve pieces are measured.

The current through the coils of the second magnet is given on the horizontal axis, whereas the intensity of the mass peaks is presented on the vertical axis. Fourteen mass peaks occur, corresponding to all possible cluster ions in the range H_3^+ to H_{29}^+. Whereas the parent mass signal (H_{29}^+) has been attenuated, the other mass peaks are produced in the scattering chamber. (Note that the maximum of the signal corresponding to the fragment ion H_{15}^+ is higher than the maximum of the H_{13}^+ and H_{17}^+ signals.)

By transferring the positions of the mass peaks relative to the current to positions relative to the magnetic field, the mass peaks become equidistant occurring at $B_{\text{fragment}} = (m(\text{fragment})/m(\text{parent})) \cdot B_{\text{parent}}$. Thus, the velocity of the fragments roughly equals the velocity of the cluster ions. Errors in determining the positions of the mass peaks relative to the current, owing to their peak forms, and in transforming the current to magnetic field strength result in an uncertainty of 5 eV in the kinetic energy of the fragments. This error is much larger than the binding energy of the H_2 molecules to the cluster ion [6]. The fact that the mass peaks have different shapes introduces a relative error in the intensities which is estimated to be 10%, in the worst cases. A second uncertainty is caused by the finite width of the detector opening in front of the second magnet. Fragments which are scattered under angles larger than the acceptance angle are not measured. A third uncertainty is caused by the transmission of the apparatus and the differing multiplier efficiencies for the different fragments. Although the error introduced in this way is yet unknown we believe it to be small. Of course, in comparing the intensities of neighbourhood mass peaks, all these errors become unimportant.

Before we discuss the quantitative results of our fragmentation measurements we will discuss the influence on the fragmentation of cluster ions of background gas molecules present even when the scattering chamber is emptied. In this situation, a background fragment intensity $I_{m,b}$ is measured on mass m, for a fixed parent mass n. Since the background pressure is constant along the beam path (2×10^{-7} torr) and since $\frac{2}{3}$ of the beam path is traversed upstream of the scattering chamber, the change of the background fragment intensity $I_{m,b} - I_{m,p}$ due to filling the scattering chamber (length l, scatter-gas density n), becomes for small attenuations

$$I_{m,b} - I_{m,p} = \tfrac{2}{3} I_{m,b} nl\sigma_m + \tfrac{1}{3} I_{m,b} nl\sigma_n \tag{2}$$

Here, σ_m and σ_n are the integral cross-sections of the fragment mass m and the parent mass n.

If $I_{m,\text{exp}}$ is the fragment intensity with the scattering chamber filled, one obtains the signal I_m due to the influence of the scatter gas alone

$$I_m = I_{m,\text{exp}} - I_{m,p} = I_{m,\text{exp}} - I_{m,b} + \frac{nl}{3} I_{m,b}(2\sigma_m + \sigma_n) \tag{3}$$

All our results were corrected using eqn. (2). In all cases this correction

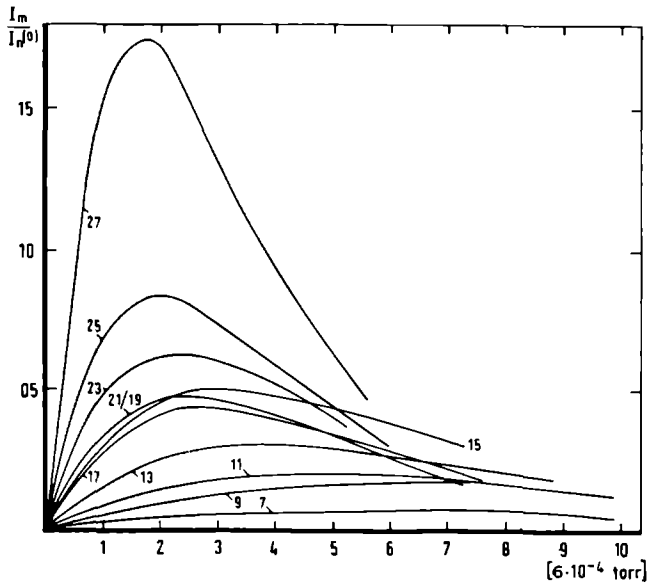

Fig. 5. Relative fragment intensities versus pressure in the scatterbox; the reading of the ion gauge was corrected by a factor of 8 for the ionization efficiency of He. The curves were taken with H_{29}^+ as parent mass, at 500-eV collision energy. The stability of H_{15}^+ is reflected by its high intensity.

introduced an uncertainty in the obtained fragmentation cross-sections smaller than 2%, although in the worst cases, $\sigma_{31,33}$, $\sigma_{29,31}$, $\sigma_{27,29}$ and $\sigma_{25,27}$, the second and third terms of the right-hand side of eqn. (3) may become comparable to I_m, at 10^{-4} torr.

Figure 5 shows the production of fragments for the cluster ion H_{29}^+ as a function of the pressure in the scattering chamber. The pressure in the scattering chamber is given on the horizontal axis and, on the vertical axis, the intensity of the fragments divided by the unattenuated intensity of H_{29}^+.

Under conditions discussed below an analytical expression can be derived for the fragment intensity as a function of the pressure in the scattering chamber. Let us define σ_n and σ_m as the integral cross-sections of the parent mass H_n^+ and the fragment mass H_m^+, σ_{mk} as the integral fragmentation cross-section for the fragmentation of H_k^+ to H_m^+, $I_k(x)$ as the intensity of the fragment ion H_k^+ at the position x in the scattering chamber and n as the helium density in the scattering chamber. The change $dI_m(x)$ of the fragment intensity $I_m(x)$ over a length dx is given by

$$dI_m(x) = I_n(x)n\sigma_{mn}dx - I_m(x)n\sigma_m dx + \sum_{k>m}^{n-2} I_k(x)n\sigma_{mk}dx \qquad (4)$$

$I_n(x)$ and $I_n(0)$ are the parent intensities at the position x and in front of the scattering chamber, respectively. We assume $I_n(x) = I_n(0)e^{-nx\sigma_n}$.

The third term on the right-hand side of eqn. (4) describes the fragmentation of fragments formed upstream of position x in the scattering chamber to mass m.

Since the first term is linear and the second and third terms quadratic in n, at sufficiently low pressures eqn. (4) reduces to

$$dI_m(x) = I_n(x)n\sigma_{mn}dx \tag{5}$$

Thus, approximately

$$I_m(l) = I_n(0)n\sigma_{mn}l \tag{6}$$

With the help of eqn. (6) the fragmentation cross-sections σ_{mn} were determined, using only the initial slope of the fragment intensity curves shown in Fig. 5.

If the fragment mass is not too different from the parent mass so that multistep fragmentation can be neglected, eqn. (4) reduces to

$$dI_m(x) = I_n(x)n\sigma_{mn}dx - I_m(x)n\sigma_m dx \tag{7}$$

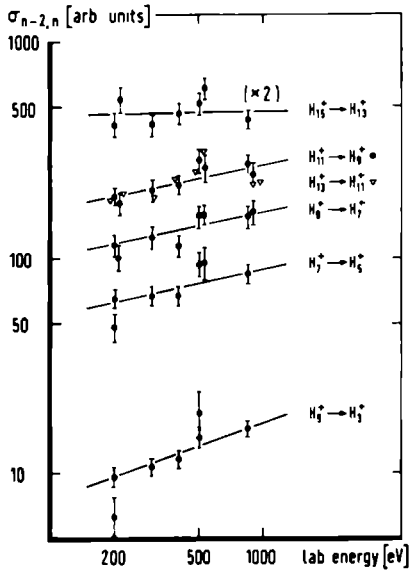

Fig. 6. The fragmentation cross-section for the loss of one H_2, versus energy. The value 100 of the ordinate corresponds to 0.35 $Å^2$. For heavier parent masses > 15 amu and also for fragmentation loss of more than one H_2, these cross-sections become energy independent.

Substituting $I_m(x) = A(x)e^{-n\sigma_m x}$ into eqn. (4) and integrating yields

$$I_m(l)/I_n(0) = -\sigma_{mn}/(\sigma_n - \sigma_m)[e^{-n\sigma_n l} - e^{-n\sigma_m l}] \quad (8)$$

Equation (8) describes Fig. 5 qualitatively as regards the form of the curves as well as the shift of the position of the maxima to larger inlet pressures for smaller fragments. Note that the experimental intensity curve of fragment mass 15 lies above the intensity curve of fragment mass 17 (this corresponds to a large $\sigma_{15,29}$-value) yielding a strong proof of the relative stability of the fragment mass 15.

The mass and energy dependence of fragmentation is presented in Fig. 6. The energy of the parent ion is given on the horizontal axis, and on the

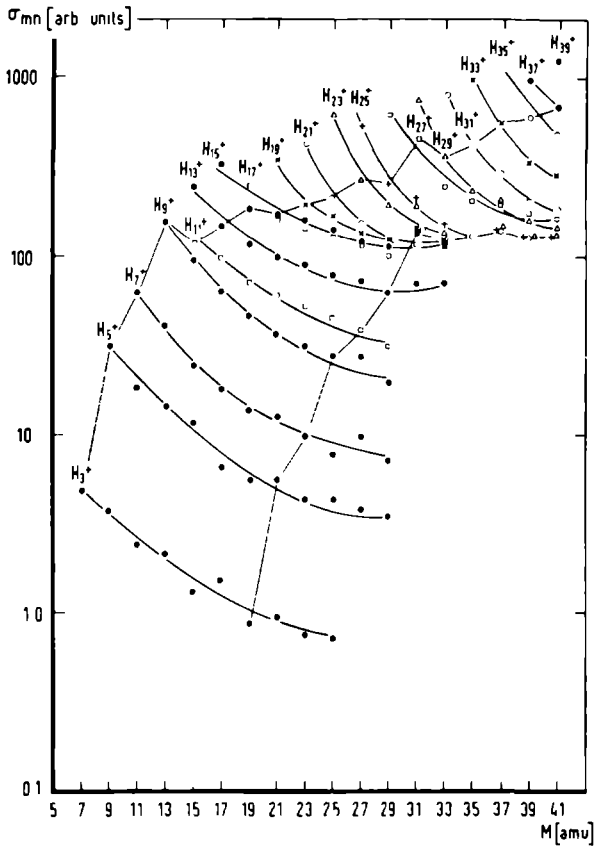

Fig. 7. The fragmentation cross-section versus parent mass, for all investigated energies. The fragment masses are indicated on top of the curves. The narrow lines correspond to $\Delta m = 4$ and $\Delta m = 16$ fragmentations. Again, $\sigma_{mn} = 100$ corresponds to 0.35 A^2.

vertical axis the fragmentation cross-sections $\sigma_{n-2,n}$. Only fragmentation cross-sections are presented with a parent mass $\leqslant 15$ amu. For $n \geqslant 15$ or $\Delta m > 2$, $\sigma_{m,n}$ becomes independent of energy within an uncertainty of 10%. Thus we are able to present all these fragmentation data obtained in the energy range 200—850 eV by energy-independent curves. The result is shown in Fig. 7, where fragmentation cross-sections are plotted versus the parent masses. The parameter of each curve gives the fragment ion considered. Following such a curve, starting from the lowest parent mass, shows how the fragmentation cross-section for that fragment behaves as a function of the parent mass.

Note the small gap between the curves belonging to fragments H_9^+ and H_{11}^+, and further that the curves corresponding to fragments H_{15}^+ and H_{17}^+ and also H_{27}^+ and H_{29}^+ nearly coincide for all parent masses. We take this as an indication that H_9^+, H_{15}^+ and H_{27}^+ are particularly stable.

In Fig. 7 the two narrow lines represent the fragmentation cross-sections $\sigma_{n-4,n}$ and $\sigma_{n-16,n}$. Following such a curve one finds that these fragmentation cross sections change by a factor 100. The $\Delta m = 14$ curve shows a sharp rise up to fragment mass-17 and becomes less steep thereafter. The same tendency is shown by the $\Delta m = 4$ curve.

Furthermore these curves show peaks for the fragment ions H_9^+, H_{15}^+ and H_{27}^+. For a more appropriate presentation of these features, see Fig. 8, where relative fragmentation cross-sections at 500 eV are presented. The mass of the fragment is given on the horizontal axis and on the vertical axis the fragmentation cross-section divided by the integral collision cross-section of the parent ion. The parameter distinguishing each curve in Fig. 8 is the number of H_2 molecules the parent ion has lost upon collision.

We see that the relative fragmentation cross-section becomes approximately independent of the parent cluster ion for $\Delta m > 6$. Furthermore, it is

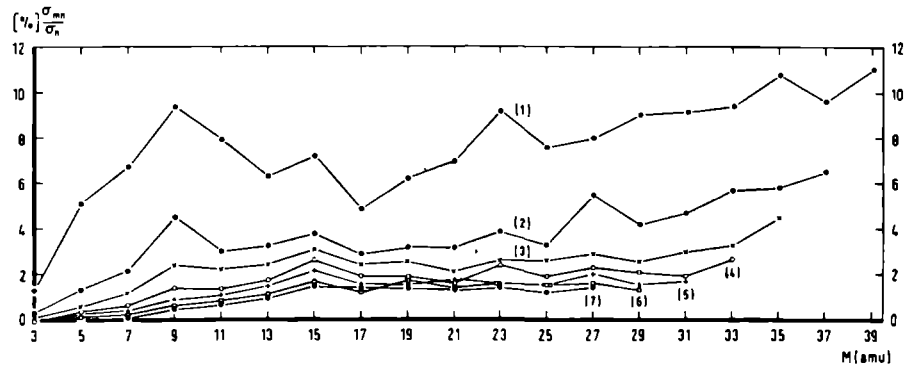

Fig. 8. Relative fragmentation cross-sections σ_{mn}/σ_n versus fragment mass M, at 500 eV. The curves correspond to $\Delta m = 2$ (1), $\Delta m = 4$ (2) etc. Peaks at stable ions are clearly displayed.

only about a factor of two more probable to scatter one H_2 molecule out of a cluster ion than two H_2 molecules. Scattering several H_2 molecules out of a cluster ion is even less dependent on the precise value of Δm. This result clearly demonstrates that fragmentation is not caused by successive scattering of H_2 molecules out of the ion. It looks more like evaporation of H_2 molecules, once one H_2 molecule is hit, and energy thus imparted to the cluster ion.

The curves for σ_{mn}/σ_n are almost horizontal except for some characteristic peaks and the behaviour for very small fragment masses. Consequently, $\sigma_{mn} \sim n$ since this behaviour is observed for σ_n, see Fig. 2. This proportionality suggests very loosely-bound cluster ions, where the H_2- molecules can be considered in first approximation as nearly equivalent, as in a droplet.

However, as can be seen from Fig. 8, fragmentation towards H_9^+, H_{15}^+ and H_{27}^+ is favoured above fragmentation towards their respective neighbours for fragment masses not too different from the parent mass. These characteristic peaks occur independently of the number of H_2 molecules lost. It clearly proves that these cluster ions are particularly stable, i.e. interesting non-droplet-like configurations exist.

Also for the fragment ions H_{19}^+ and H_{23}^+ indications of relative stability compared to their neighbours are observed in Fig. 8.

DISCUSSION

From the relative intensities of cluster ions, when a nozzle beam is ionized by electron bombardment, but especially from relative fragmentation cross section measurements strong evidence is gathered for the existence of particularly stable H_9^+, H_{15}^+ and H_{27}^+ ions. For all three ions, symmetric configurations can be suggested: H_9^+ forms an equilateral triangle H_3^+ surrounded by three H_2-molecules positioned on the three middle lines through the corners of the triangle as discussed in ref. 6; H_{15}^+ an octahedron with the H_3^+ in its centre and six H_2 molecules in its corners; H_{27}^+ an icosahedron with H_3^+ in its centre, ten H_2 molecules forming pentagons in planes above and below this centre and one H_2 molecule at top and bottom (see ref. 8). Preparations of measurements for larger clusters are in progress.

REFERENCES

1 A. van Lumig and J. Reuss, Int. J. Mass Spectrom. Ion Phys., 25 (1977) 137.
2 R. Clampitt and L. Gowland, Nature, 223 (1969) 815.
3 R. Clampitt and J.D. Jefferis, Nature, 226 (1970) 141.
4 K. Buchheit and W. Henkes, Z. Angew. Phys., 24 (1968) 191.
5 A. van Deursen and J. Reuss, Int. J. Mass Spectrom. Ion Phys., 11 (1973) 483.
6 K. Hiraoka and P. Kebarle, J. Chem. Phys., 62 (1975) 2267.
7 W.I. Salmon and R.D. Poshusta, J. Chem. Phys., 59 (1973) 4867.
8 J. Easterfield and J.W. Linnett, Chem. Commun., 64 (1970).
J.T. Huang, M.E. Schwartz and G.V. Pfeifer, J. Chem. Phys., 56 (1972) 755.
8 R.D. Etters, R. Danilowicz and J. Dugan, J. Chem. Phys., 67 (1977) 1570.
9 H.U. Mittmann, H.P. Weise, A. Ding and A. Henglein, Z. Naturforsch. A, 26 (1971)
40 1112, 1122 and 1282.

Double differential fragmentation cross section measurements of H_{2n+1}^{+} ions, $n \leq 7$

A. van Lumig and J. Reuss

Fysisch Laboratorium

Katholieke Universiteit

Nijmegen, The Netherlands

and

A. Ding, J. Weise and A. Rindtisch

Hahn-Meitner-Institut

West-Berlin, Germany

Summary

Pursuing previous integral fragmentation cross section measurements of hydrogen cluster ions with He as scattering partner (ref. 1), double differential fragmentation cross sections against Ar have been measured for ions in the mass range from H_5^+ to H_{15}^+.

The ions are formed by electron bombardment of neutral clusters in a nozzle beam and extracted from the ionizing region at an energy of 300 eV; right in front of the scattering region they are decelerated to a laboratory energy E_0 between 6.8 and 75 eV. In the scattering region the primary (parent) ion beam is attenutated and fragment (daughter) ions are formed. The detection of the parent and daughter ions occurs as function of their laboratory deflection angle as well as their laboratory velocity.

It is found that both the angle distribution and the velocity distribution broaden symmetrically with an increase of the number of H_2 molecules lost in the fragmentation process. For example, at an energy E_0 = 6.8 eV the values for the FWHM of the angular distributions in case of H_{13}^+ and H_5^+ (parent ion H_{15}^+) amount to 1.8° and 8.4°, respectively. The FWHM for the velocity distributions are 200 m/s and 1500 m/s, respectively. Except for the fragment H_5^+ from parent H_{15}^+ and H_{13}^+ where a 5% shift to lower velocities is observed at E_0 = 6.8 eV the mean velocity of the other fragment ions equals the velocity of their parent ion, within the experimental accuracy of 2%.

The measured fragment angle distributions (proportional to $d\sigma_{m,n}/d\Omega$) are converted to $I_{m,n}(\theta)$-curves (proportional to $d\sigma_{m,n}/d\theta$) by multiplication with sin θ. For Ar and H_2 as scattering partner it is found that the normalized distributions $I_{m,n}(\theta)$ follow a universal curve if plotted against $\theta\sqrt{E_0}$. Further, the FWHM of the time of flight measurements (TOF) decreases

proportional to E_0^{-1}. From both these findings we shall argue that, in a system travelling with the cluster, the fragments are distributed independently of E_0.

A broadening of the angle distribution of the attenuated parent ions is hardly noticable. The total sum of the integrated fragment intensities equals the loss of intensity of the parent ion, within the experimental accuracy of 20%. Both observations lead to the conclusion that elastic scattering is unimportant.

1. Introduction

Integral total and fragmentation cross sections of H_{2n+1}^+ ions ($n \leqslant 20$) colliding with N_2 and He were reported, recently (ref. 1, 2). We became interested in angle and velocity distributions, too, in order to get a better understanding of cluster ion fragmentation processes.

Stable configurations have manifested themselves in preferential fragmentation to certain fragment masses (e.g. H_3^+) (ref. 1). It seemed worthwhile to investigate whether stable configurations influence, too, the angle and energy distributions.

The results presented in ref. 1 and 2 were obtained with the detector at a fixed position and with an acceptance angle of about 10^{-4} sterad. The influence of the small detector opening, especially upon the fragmentation cross section results could not be determined, at that time. With the present measurements this gap is filled, too.

For small ions (e.g. H^+ and H_2^+) rainbow structures have been resolved clearly (ref. 3, 4, 5, 6). From the rainbow structure, the depth of the potential can be determined. Our attempt to discover similar rainbow maxima for H_3^+, H_5^+, etc. (colliding with He, Ne, Ar, Kr, Xe, H_2, and CO_2) was futile, although the same apparatus was used and the ion beam quality was equally

good as in ref. 3, 4, 5. Probably, angle dependent forces smear out a possible rainbow structure in case of H_3^+, whereas fragmentation processes dominate the interaction for larger cluster ions, so that elastic potential scattering with its rainbow phenomenon is not apt to describe the situation.

Double differential cross section measurements, for example using the TOF technique are widely used to draw conclusions concerning the reaction mechanism (ref. 7, 8, 9). If a long lived excited complex is involved in the reaction, a shift of the average fragment velocity occurs, from which the excitation energy can be determined. From our measurements would follow an excitation energy for instance of (0.7 $\pm$ 0.4) eV for parent mass H_{15}^+, fragment mass H_5^+ and E_0 = 6.8 eV.

The observed angle distributions allow an estimate of how much energy is carried off as kinetic energy, on the average, by an H_2 molecule leaving the parent ion. Except for the directly hit H_2 molecule, the other ones are assumed to evaporate in a random manner. Upon leaving the complex each one impacts a recoil momentum on the fragment opposite to its own momentum. Consequently, the fragment ions show an angle and energy distribution revealing the average momentum of the H_2 molecules.

2. Apparatus

The apparatus is sketched schematically in Fig. 1. It is equipped with a cluster ion source described in ref. 1. This source has been mounted on a differential ion scattering machine of the Hahn-Meitner-Institut at West-Berlin, which is described in ref.10. For the present purpose, only the essential features are repeated.

The ions formed at the ionization region I (Fig. 1) are accelerated to an energy of 300 eV by the ionizer lenses. At this energy they travel a dis-

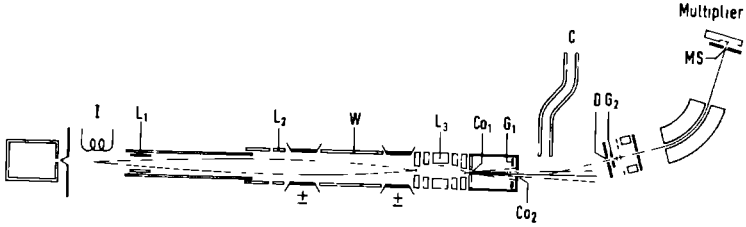

Fig. 1. The apparatus. The cluster ions are accelerated to an energy of 300 eV immediately after the ionization region I. The beam is focused by two electrostatic lenses L_1 and L_2, mass selected by Wien filter W and decelerated at L_3. Ater collimation by Co_1 and Co_2, the beam passes the scattering region. At the detector, the ions are again accelerated, mass analyzed and fed into a particle multiplier. The detector rotates around the scattering region. For TOF measurements, two pairs of deflection plates G_1 and G_2 are inserted which determine the length of the TOF path.

tance of about 120 cm, on their way being focused by two electrostatic cylindrical lenses L_1 and L_2. The Wien filter W is transparent only for a single variable ion mass. Behind the Wien filter the ions are decelerated and focused by a lens system L_3 due to Menzinger (ref. 11). Next, two collimator holes Co_1 and Co_2, 8 cm apart and 0.5 mm in diameter, reduce the divergence of the primary beam. At an energy of 6.8 eV the divergence of the beam amounts to about 1.6° FWHM. It decreases slowly with increasing energy and amounts to about 0.5° at 75 eV ion energy. For H_{15}^+, the value for the FWHM of the measured TOF distribution amounts to about 0.7 μs at

an energy of 6.8 eV (flight time 44 μs) and decreases to about 0.25 μs at 75 eV energy (flight time 13.4 μs).

The ion beam is attenuated with the help of a secondary beam effusing from a 1.5 mm wide horizontal capillary C which is mounted next to the primary beam within a distance of 0.5 mm. The dimensions of the scattering volume are quite small relative to the distance between scattering region and detector so that nearly point source scattering is achieved. Normally, an attenuation by a factor two was realized for the primary cluster ion beams.

The detector opening D (3 mm diameter) is reached 400 mm downstream the collimator hole Co_2. The acceptance angle amounts to about 5×10^{-5} sterad. The maximum intensity of the primary ion beam within this acceptance angle amounts to a few times 10^6 particles/s, more or less independent of the ion energy and mass of the cluster ion. The maximum fragment intensities range from 2×10^4 down to 500 particles/s.

The distance between D and Co_2 is carefully shielded to prevent electrical fields to disturb the ion beam. The detector is movable in the horizontal plane (spanned by the primary and the secondary beam) around the scattering centre. At the detector the ions are accelerated by a lens system to an energy of a few hundred eV to allow second mass analysis by a magnet. The mass resolution of this magnet is kept low inserting a wide MS slit of about 10 mm; this is important to prevent discrimination between particles of the same mass but different velocities. The mass resolution $m/\Delta m$ amounts to about 10 and limits the mass range investigated to masses not larger than H_{15}^+.

Detection of the particles occurs by an open electron multiplier (type Bendix M306); particle counting techniques are employed.

Two pairs of deflection plates G_1 and G_2 are inserted behind the deceleration lens system and behind the detector opening to interrupt the ion

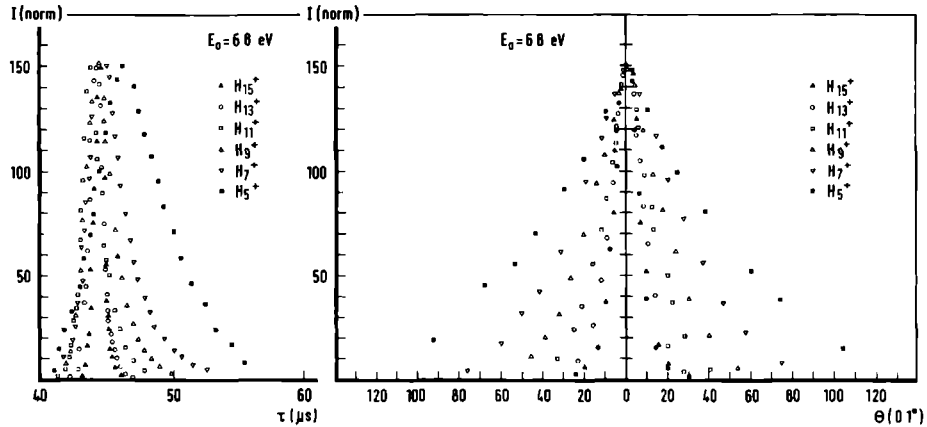

Fig. 2, 3. TOF and angle distribution results at 6.8 eV, normalized to equal height, are presented for parent mass H_{15}^+ and its fragment masses H_{13}^+ down to H_5^+. The scatter gas is argon. No significant difference was observed between TOF measurements at different deflection angles. The curves broaden symmetrically with increasing fragmentation. Only for fragment mass H_5^+ a shift in the time of arrival is observed of about 5%. Notice that the curves for the primary (▲) and the attenuated (●) parent mass nearly coincide.

beam for the TOF measurements. The flight time can be accurately determined thus over a length of 42.0 ± 0.4 cm. It turns out that the ion energy calculated from the time of flight results differs from the direct voltage reading by about 30% at low energies, because of charging of the lens elements and space charge effects, probably.

3. Results

In Fig. 2 and 3, results of TOF measurements in forward direction and angle distribution measurements are shown for H_{15}^+ and its fragments at an energy E_0 = 6.8 eV, with argon as secondary beam gas. On the horizontal axis the flight time in forward direction (in μs, Fig. 2) and the deflection angle θ (in degrees, Fig. 3) are given, respectively. On the vertical axis the measured intensities are given, normalized to equal maximum height. With the secondary beam turned off, on the fragment masses no ion signal was detected due to background gas scattering in excess of the background noise of about 10 particles/s.

The measured TOF distributions are practically independent of the laboratory deflection angles ($\theta \leq 10^o$).

By means of measurements like those presented in Fig. 2 (but for various detector angles) and Fig. 3 flux-velocity-angle-contour maps are computed for the lab system, giving a complete picture of the processes studied. In Fig. 4 maps are plotted for unattenuated and attenuated H_{15}^+ and all fragment beams H_{13}^+ to H_5^+. Similar plots have been obtained for all fragmentation processes, starting at smaller cluster size and/or higher energy.

The radial distance $(v_x^2 + v_y^2)^{\frac{1}{2}}$ corresponds to the lab velocity of the cluster ions, whereas the indicated angle coordinate (v_y/v_x = constant lines) represents the laboratory deflection angle. The numbers indicate contour lines of the normalized ion intensity (maximum = 100).

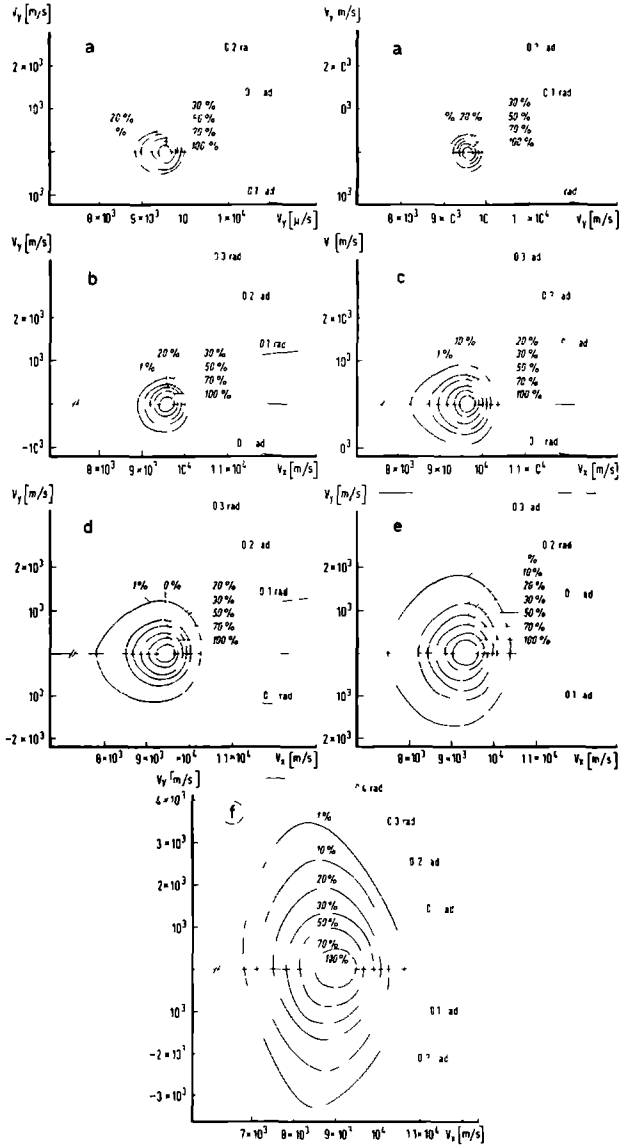

Fig. 4. Contour intensity diagrams for primary (a) and attenuated (a') parent mass H_{15}^+ and fragment mass H_{13}^+ down to H_5^+ (b-f), at 6.8 eV. The large influence of the number of H_2 molecules, lost by the fragmentation process, is clearly demonstrated.

Notice the fact that tne velocity at intensity 100 in case of fragment ion H_5^+ is shifted to lower velocities by about 5% compared to the corresponding velocity of parent ion H_{15}^+. Within an accuracy of about 2% all other fragment masses have retained the original velocity of the unattenuated H_{15}^+ beam, at intensity 100.

With increasing fragmentation the contour lines broaden with respect to the angular and the velocity coordinate, a feature we ascribe to the increasing number of recoils experienced by the smaller fragments during evaporation of H_2 molecules. The velocity broadening amounts to 1500 m/s FWHM at most, i.e. 16% of the incoming velocity at 6.8 eV, the angle broadening to 8.4^o FWHM, at most.

Two experimental features have to be mentioned. Each time the secondary beam was switched on the primary beam has been refocused, for small E_0 at least, by L_2 (40 cm in front of the secondary beam capillary, see Fig. 1). At 6.8 eV and to a lesser extent at 17 eV lab energy this refocusing results in a narrowing of the angular distribution. We believe that the target gas has influence upon the beam width, possibly by space charge effects. We refocuse the attenuated beam to have a beam as narrow as possible and consequently the primary beam width has lost its exact definition. Accidently, at 6.8 eV we even have worked sometimes with a 20% narrower attenuated beam as compared to the unattenuated beam. At higher energies this refocusing has not been applied; no beam broadening was observed.

A second experimental uncertainty is present in the TOF measurements. The TOF spectrum of the primary ion beam changes during the measurements, possibly due to defocusing influence by space charge. At least partly, the asymmetry of the maps in Fig. 4 is caused by this drift; only the low velocity side of the TOF spectrum is affected; by readjusting the lens voltages of L_2 this broadening has been reduced between the measurements.

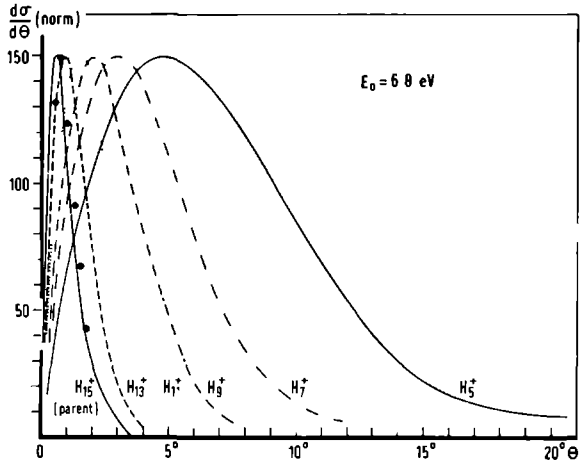

Fig. 5. $I_{m,15}(\Theta)$-curves, normalized to equal height, for $m \leq 15$ at an energy of 6.8 eV. The dots represent the primary parent mass; the full line represents the atteruated parent mass.

4. Analysis of angle distributions

In Fig. 3 the angle dependence of the fragment intensities is shown for parent mass H_{15}^+ at an energy of 6.8 eV. We have varied the density of the secondary beam but no influence upon the normalized angle distributions has been observed. The densities thus tested range from very low values up to a value five times larger than the density at which the measurements of Fig. 3 are performed. Apparently, multiple collision processes dit not produce an angular distribution differing from those caused by single scattering.

It also follows that the measured fragment intensity curve is proportional to the $d\sigma_{m,n}/d\Omega$-curve for the fragmentation process. The curves are symmetric around the primary beam direction; from this symmetry we infer that the results are independent of the azimuth angle around this direction, as one can expect from the very small velocity of the target molecules.

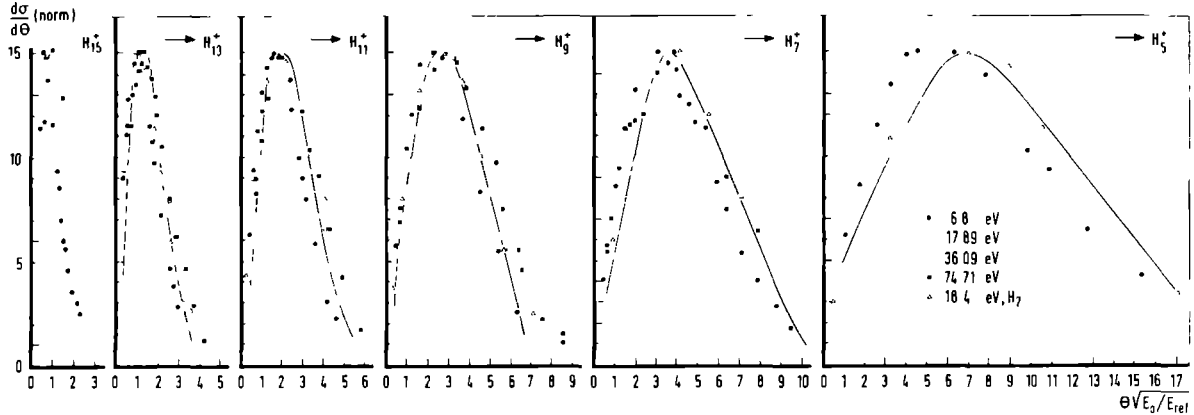
dσ/dΘ (norm)
H15+
H13+
H11+
H9+
H7+
H5+
6 8 eV
17 89 eV
36 09 eV
74 71 eV
18 4 eV, H7
ΘVE0/Eref

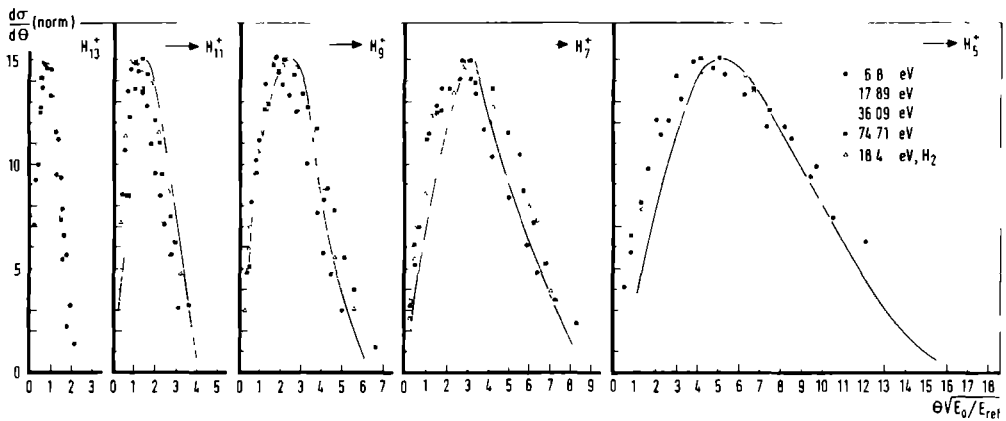
dσ/dΘ (norm)
H13+
H11+
H9+
H7+
H5+
6 8 eV
17 89 eV
36 09 eV
74 71 eV
18 4 eV, H2
ΘVE0/Eref

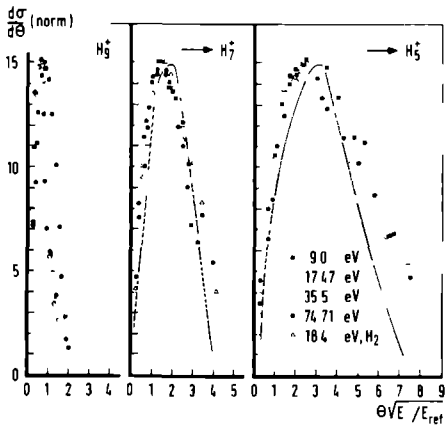

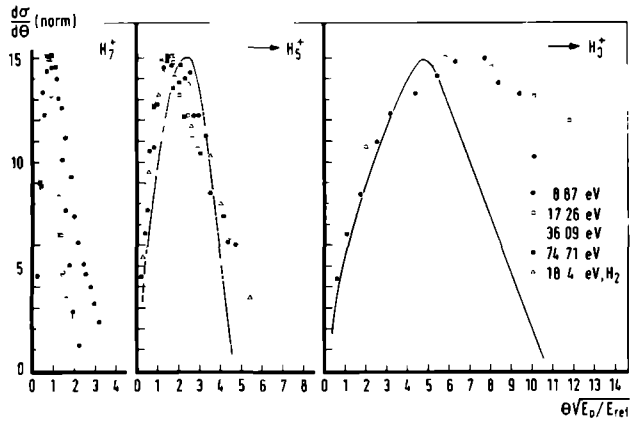

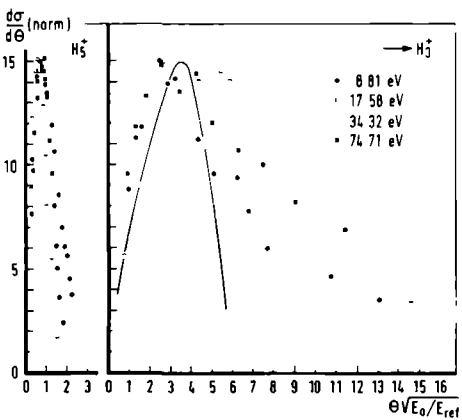

Fig. 6. Reduced $I_{m,n}$ curves, normalized to equal height, for $n \leqslant 15$ and $m \leqslant n$. The reference energy E_{ref} is put equal to 6.8 eV (parent ion H_{15}^+ and H_{13}^+) and about 8.8 eV (parent ion H_9^+, H_7^+ and H_5^+). By △ results are presented for the scattering against H_2 as secondary beam gas, at 18.4 eV. The drawn lines correspond to the results of model calculations for the fragment angle distributions.

Then, $d\sigma_{m,n}/d\theta$ equals $(d\sigma_{m,n}/d\Omega)\sin\theta 2\pi$, where again θ represents the deflection angle. In Fig. 5, $I_{m,n}(\theta)$-curves ($I_{m,n}(\theta) \sim (d\sigma_{m,n}/d\Omega)\sin\theta 2\pi$) for parent ion H_{15}^+ at 6.8 eV are displayed with the peak intensity normalized to equal height. Corrections due to the finite opening of the detector (3 mm ∅; 400 mm downstream the scatter region) are only important for deflection angles smaller than 0.2°.

Similar curves are obtained for other parent masses and other energies up to 75 eV. At a given parent mass and energy the position of the maximum of $I_{m,n}(\theta)$ shifts to larger angles with increasing fragmentation, e.g. the maximum of H_{13}^+ (parent ion H_{15}^+) is found at 1.1° and of H_5^+ (parent ion H_{15}^+) at 5.0°, at a primary ion energy of 6.8 eV (Fig. 5).

For a fixed fragmentation (for instance, $H_{2n+1}^+ \rightarrow H_{2n-1}^+$) the position of the maximum shifts to smaller angles with increasing n, e.g. the maximum of H_{13}^+ (parent ion H_{15}^+) is found at 1.1° for E_0 = 6.8 eV (Fig. 5) whereas the maximum of H_5^+ (parent ion H_7^+) is found at 1.7° (Fig. 6), even at a higher energy E_0 = 8.87 eV.

In Fig. 6 it is shown that we obtain unique $I_{m,n}$-curves for the whole range 6.8 - 75 eV for each fragmentation process with m > 3 by a plot against $\theta\sqrt{E_0/E_{ref}}$ instead of θ. For each E_{ref} we always take the lowest used ion energy (see Fig. 6).

The influence of the primary distribution on the results displayed in Fig. 6 decreases for larger fragmentation; it amounts to about 50% for $H_{15}^+ \rightarrow H_{13}^+$ and to about 10% for $H_{15}^+ \rightarrow H_5^+$. Fortunately, this influence also scales roughly with $\theta\sqrt{E_0/E_{ref}}$ (see primary beam distributions in Fig. 6).

In Fig. 6 results also are shown obtained from measurements with H_2 as secondary beam gas (E_0 = 18.4 eV). Notably the $\theta\sqrt{E_0/E_{ref}}$ reduction again leads to the unique $I_{m,n}$-curves obtained for Ar.

The reduction of the fragment intensity curves with $\theta\sqrt{E_0/E_{ref}}$ suggests

that the angle distributions are caused by a fragmentation process independent of the primary energy if viewed by an observer travelling with the velocity of the primary beam. A simple model containing this feature describes approximately the angle dependence for all parent and fragment masses. The H_2 molecules which leave the cluster ion upon collision are assumed to be distributed randomly. For their average kinetic energy the value of (0.05 ± 0.01) eV is found to describe the angle distributions; this value is independent of parent mass, fragment mass and energy E_0. By a Monte Carlo simulation the angle distributions are readily obtained. A two dimensional example of such a random walk scheme (for H_{15}^+ fragmentating to H_5^+ at 6.8 eV) is shown in Fig. 7. The parent ion H_{15}^+ is assumed to travel in forward direction. Before the evaporation of the first H_2 molecule, the momentum P_A of the H_{13}^+ fragment (mass m_A) amounts to m_A/m_B

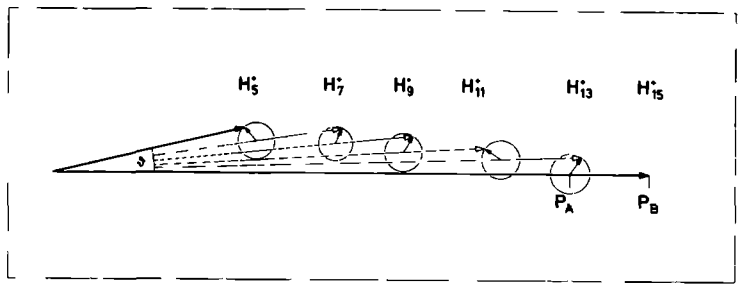

Fig. 7. Two dimensional example of a random walk scheme in case of parent ion H_{15}^+ fragmentating to H_5^+, at 6.8 eV. The momentum of fragment H_{13}^+, before the evaporation of the first H_2 molecule has occurred, amounts to 13/15 times the momentum of parent ion H_{15}^+. The recoil (momentum of fixed absolute value, but of random direction) of the ejected H_2 molecule changes the momentum of the H_{13}^+ ion, and so on.

times the momentum P_B of parent ion H_{15}^+ (mass m_B). The recoil (momentum of fixed absolute value, but of random direction) of the ejected H_2 molecule changes the momentum of the H_{13}^+ ion. Continuing the calculations to $H_{.1}^+$, the momentum of the H_{13}^+ fragment is used to calculate the initial momentum of fragment H_{11}^+ (see Fig. 7), and so on for all other parent and fragment ions. In Fig. 6 the results of the best fit to the measurements are shown. Using the primary distribution at E_0 = 36 eV the fragment distributions are calculated and presented in $0\sqrt{E_0/E_{ref}}$ units. Except for the evaporation of a single H_2 molecule, we see that the measurements are described rather well. The value for the average kinetic energy (0.05 eV) is comparable to the binding energies of the cluster ions (ref. 12, 13). No significant deviations from the simple model calculations are found for fragment H_9^+ in spite of its high stability.

5 Integral fragmentation cross section

As discussed above, at low energies (6.8 eV) the primary angle distribution is affected by the secondary beam, probably due to space charge effects. At higher energies ($\geq$ 36 eV) this effect is absent. Comparison between the primary angle distribution and the attenuated distribution (normalized to the same height) then shows that both are equal within 0.05^o or less, although an attenuation of a factor two is applied. This result is consistent with the assumption that the attenuation of the primary beam is mainly caused by the fragmentation processes.

Integration of the $I_{m,n}(0)$-curves like those in Fig. 5 and removing their normalization yields the total fragment intensity for given parent mass n and fragment mass m, for the attenuation applied. The sum of these intensities for all fragment masses at a given parent mass equals the loss of intensity of that parent mass within the uncertainty of 20%.

This result and the unchanged angle distributions for the parent mass show that indeed elastic scattering processes can be neglected. Shadow scattering (ref. 14) with its spacing of maxima of about $1^{\circ}/\sqrt{E_0}$ is not resolved (E_0 in eV).

From these fragment intensities relative values for the fragmentation cross section can be found. We have reported earlier (ref. 1) how parent and fragment intensity depend on the density of collision partners in a scattering chamber for energies between 200 and 850 eV. In case of parent ion H_{15}^+ these results are reproduced in a slightly different form in Fig. 8; on the horizontal axis the ratio I/I_0 of attenuated and unattenuated intensity is plotted; on the vertical axis $I_{m,15}\,(I/I_0)/I_{m,15}\,(0.5)$ is given.

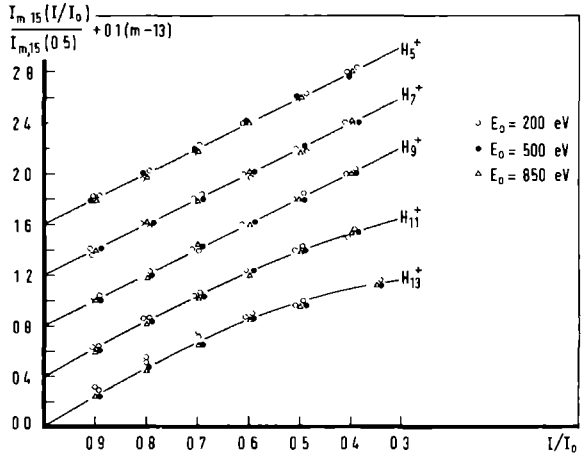

Fig. 8. Fragment intensity curves $I_{m,15}(I/I_0)/I_{m,15}(0.5)$, obtained at 200, 500 and 850 eV, versus the attenuation I/I_0 of parent mass H_{15}^+.

For example, only if $I/I_0 \geq 0.8$ the fragment intensities in case of parent ion H_{15}^+ and fragment ion H_{13}^+ are proportional to $\sigma_{m,n}$ (ref. 1). The correction for nonlinearity to be applied at a given I/I_0 ratio to obtain the true value for the $\sigma_{m,n}$, appears to be independent of the ion energy for this energy range. This experimental finding is supported by Eq. (8) in ref. 1, that takes into account the most important corrections upon the fragmentation cross section due to a too large attenuation. We take the correction factors from Fig. 8 (obtained in the energy range 200-850 eV) to apply also in the present energy range of 6.8 to 75 eV.

In case of $H_{15}^+ \rightarrow H_{13}^+$ at an I/I_0 ratio of 0.5 we obtain a nonlinearity correction factor of 1.4 ± 0.1. In all other cases smaller corrections have to be carried out. For instance, for $H_{15}^+ \rightarrow H_{2n+1}^+$ a correction is practically absent ($\leq 10\%$), $n \leq 4$ and $I/I_0 = 0.5$.

In Table 1, the results for $\sigma_{m,n}$, $n = 15, 13$, $m < n$, are presented for an energy of 6.8 eV. Each entry consists of the nonlinearity correction factor in parenthesis together with the corrected value for the fragmentation cross section obtained from angle integration of the $I_{m,n}(\theta)$-curves.

Table 1. Fragmentation cross sections for parent mass H_{15}^+ and H_{13}^+, obtained from the differential measurements. The correction factor, due to the too large attenuation, is given in parenthesis.

	13	11	9	7	5
$\sigma_{m,15}$	2.2 ± 0.5	1.3 ± 0.2	4.3 ± 0.5	2.9 ± 0.3	3.3 ± 0.5
	(1.4 ± 0.1)	(1.2 ± 0.1)	(1.0 ± 0.1)	(1.0 ± 0.1)	(1.0 ± 0.1)
$\sigma_{m,13}$		2.4 ± 0.5	4.0 ± 0.6	3.3 ± 0.4	3.3 ± 0.7
		(1.2 ± 0.1)	(1.0 ± 0.1)	(1.0 ± 0.1)	(1.0 ± 0.1)

Notice the large cross sections for H_9^+. This result is consistent with earlier findings (ref. 1) and points to the relatively high stability of H_9^+. However, this stability is of no significant influence on the angle distribution.

In general terms, all fragments (except for the slight predominance of H_9^+) are equally likely to appear in the fragmentation process.

6. Time of flight measurements

In Fig. 2 TOF results are presented for parent mass H_{15}^+ at 6.8 eV energy. From these measurements the energy of the cluster ions can be accurately determined. It turns out that the average velocity of fragment ion H_5^+ is about 5% smaller than the average velocity of parent ion H_{15}^+. For the larger fragment masses this shift is not observed within the experimental accuracy of 2%. In case of fragment ion H_5^+, if formation of an excited intermediate cluster ion H_{15}^+ preceeds fragmentation by evaporation, the internal energy of excitation amounts to (0.7 ± 0.4) eV, i.e. 10% of the primary ion energy of 6.8 eV. For the larger fragment masses the excitation energy amounts to 0.4 eV at most. Such internal energies are sufficient to strip off about six H_2 molecules whose binding energies range from 0.01 eV to 0.3 eV (ref. 12, 13); the kinetic energy of each H_2 molecule amounts to 0.05 eV (see section 4).

The TOF distribution is sensitive to the number of H_2 molecules evaporated. With increasing fragmentation the TOF spectrum broadens almost symmetrically (Fig. 2). For example, the FWHM of the spectrum in case of $H_{15}^+ \rightarrow H_5^+$ is 7 μs at an average drift time of 44.4 μs at 6.8 eV. For a fixed fragmentation (for instance $H_{2n+1}^+ \rightarrow H_{2n-1}^+$) the TOF spectrum narrows with increasing n.

With increasing primary energy the width of the TOF spectra is propor-

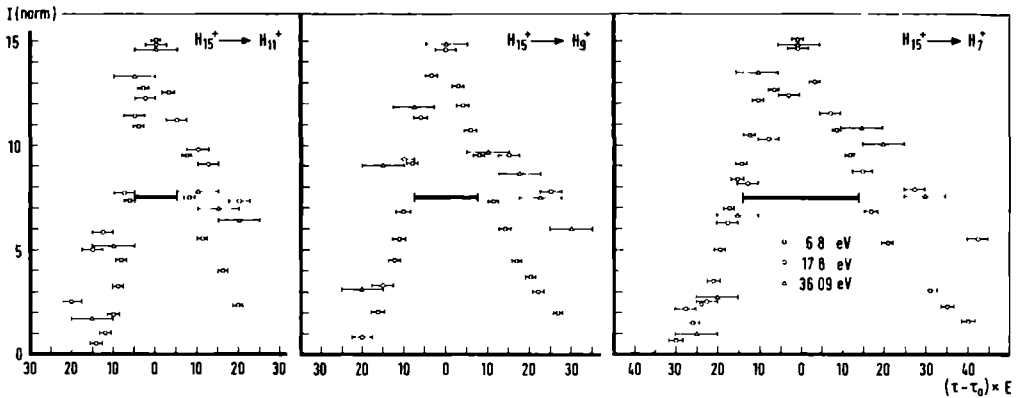

Fig. 9. Reduced TOF results for E_0 = 6.8 (□), 17.8 (○) and 36.09 (△) eV (normalized to equal height) for parent mass H_{15}^+ and a number of its fragment masses. The position of the maximum occurs at τ_0, being different for all energies. The relative flight time $\tau-\tau_0$ is multiplied by the initial energy E_0. The error bar represents the time resolution of the TOF measurements. The thick bar results from model calculations.

tional to v_0^{-2}. This result is consistent with the finding (see section 4) that the fragment recoil energy is independent of the primary energy. At an energy E_0 we measure a velocity distribution around v_0 for a given fragment mass. In general, the width at half maximum will be Δv_1 with respect to the higher velocity side and Δv_2 with respect to the lower velocity side. Then, the FWHM time difference $\Delta\tau$ of arrival for both velocities yields $\Delta\tau = l[(v_0 - \Delta v_2)^{-1} - (v_0 + \Delta v_1)^{-1}] \approx l(\Delta v_1 + \Delta v_2)/v_0^2$. Here, l is the distance between both sets of deflection plates (see section 2). The experimental results show $\Delta v_1 \approx \Delta v_2$ = constant, i.e. a symmetrical broadening proportional to v_0^{-2}. The simple evaporation model already employed to explain the angle distribution (see section 4) serves equally well to describe the TOF broadening. For this purpose we assume that 1/6 of the momentum (corresponding to the average kinetic energy of 0.05 eV) is imparted to the cluster fragment in forward or backward direction upon evaporation of a single H_2 molecule. In this way TOF-FWHM's are obtained in full agreement with the experimental results (see Fig. 9).

In Fig. 9 TOF spectra are shown in a reduced form for fragmentation processes of the parent ion H_{15}^+. The maxima of the spectra obtained at different ion energies, are shifted to coincide. Next, the flight time is multiplied with E_0. The TOF distribution for the parent ion is not accounted for. Fortunately, this distribution narrows rapidly with increasing energy. The reduced curves show general agreement (within the finite time of resolution of 0.125 μs) except at the low velocity side. There, the space charge effects discussed in section 3 render the measurements less reliable.

7. Integral fragmentation cross sections revisited

In an earlier paper (ref. 1), dealing especially with the stability of

cluster ions, we presented integral fragmentation cross sections, too. The results were obtained with the detector in a fixed position and a fixed acceptance angle of about 10^{-4} steral. The ion energy range from 200 eV to 850 eV was investigated. As scattering partner He was used. The integral fragmentation cross section results for parent mass H_{15}^+ showed a decrease of a factor 20, going from fragment mass H_{12}^+ to fragment mass H_5^+.

The reason for the discrepancy with our present results stems from the small acceptance angle during the earlier measurements. If we assume the scaling of the angle distribution with $\theta/\sqrt{E_0}$ to be valid also for the energy region of 200 eV to 850 eV and for collisions with He (in section 4 the same distribution was found for Ar and H_2, moreover, the evaporation model presupposes independence of the nature of the scattering partner) and if we take the primary distribution exactly in forward direction we can calculate the angle distribution using the evaporation model discussed in section 4. The correction, to take into account the fragments which have missed the detector in ref. 1, is displayed in table 2. Each entry comprises the correction factor and the new result for the fragmentation cross section.

The uncertainties for the correction factors of table 2 are calculated from the angular distribution of the unattenuated beam. We know that the horizontal FWHM was about 2 mm, i.e. one half of the horizontal acceptance angle. In the vertical direction we estimate that the unattenuated beam divergence leads to a FWHM about equal to or smaller than the detector acceptance. Assuming equal probability within both FWHM's yields the shown uncertainties. In table 2 the uncertainty of the corrected cross section includes the original error of ref. 1. Also at this higher energy, the corrected fragmentation cross section becomes rather independent of the fragment mass. Applying the correction, H_9^+ excels again by its large fragmentation cross section.

Table 2. Fragmentation cross sections for parent masses with $7 \leq n \leq 15$ obtained from integral measurements presented in ref. 1. The correction factor, due to the finite detector opening, is given in parenthesis.

	13	11	9	7	5
$\sigma_{m,15}$	3.4 ± 0.4	2.6 ± 0.3	3.5 ± 0.4	1.8 ± 0.2	1.6 ± 0.2
	(1.3 ± 0.1)	(2.0 ± 0.1)	(3.1 ± 0.1)	(7.0 ± 0.2)	(21.7 ± 0.4)
$\sigma_{m,13}$		3.6 ± 0.4	4.0 ± 0.5	1.7 ± 0.2	1.4 ± 0.2
		(1.5 ± 0.1)	(2.5 ± 0.1)	(4.2 ± 0.2)	(13.0 ± 0.3)
$\sigma_{m,11}$			5.0 ± 0.6	2.1 ± 0.2	1.6 ± 0.2
			(1.8 ± 0.1)	(3.0 ± 0.1)	(8.2 ± 0.2)
$\sigma_{m,9}$				3.2 ± 0.4	1.5 ± 0.2
				(2.2 ± 0.1)	(4.5 ± 0.2)
$\sigma_{m,7}$					2.4 ± 0.3
					(2.6 ± 0.1)

From the differential measurements (Fig. 6), we learn that for a fixed number of H_2 molecules evaporated, the width of the angle distribution for these fragment masses decreases with increasing parent mass. Extending the calculations to larger cluster masses, we find that the fragmentation cross sections for parent mass H_{25}^+ and larger to fragment masses involving evaporation of a single H_2 molecule need no correction any more, even at 200 eV.

Acknowledgements

This work is part of the research program of the "Stichting voor Fundamenteel Onderzoek der Materie (F.O.M.)" and has been made possible by financial support from the "Nederlandse Organisatie voor Zuiver Wetenschappelijk Onderzoek (Z.W.O.)".

Dr. Eisele has contributed by computing the contour maps (Fig. 4).

We thank Mr. Lehmann for his technical assistance.

References

1. A. van Lumig and J. Reuss, nt.J.Mass Spectrom.Ion Phys. 27 (1978) 197
2. A. van Lumig and J. Reuss, nt.J.Mass Spectrom.Ion Phys. 25 (1977) 137
3. A. Ding, J. Karlau and J. ise, J.Chem.Phys. 65 (1976) 2544
4. H.U. Mittmann, H.P. Weise, .. Ding und A. Henglein, Z.Naturforsch. 26a (1971) 1112
5. H.P. Weise, H.U. Mittmann, .. Ding und A. Henglein, Z.Naturforsch. 26a (1971) 1122
6. H.U. Mittmann, H.P. Weise, A. Ding und A. Henglein, Z.Naturforsch. 26a (1971) 1282
7. A. Henglein, K. Lackmann und G. Jacobs, Ber.Bunsenges.Physik.Chem. 69 (1965) 279
8. K. Lackmann und A. Henglein, Ber.Bunsenges.Physik.Chem. 69 (1965) 286
9. K. Lackmann und A. Henglein, Ber.Bunsenges.Physik.Chem. 69 (1965) 292
10. J. Karlau, Thesis, Technische Universität, Berlin (1977)
11. M. Menzinger and L. Wählin, Rev.Sci.Instrum. 40 (1969) 102
12. S.W. Harrison, L.J. Massa and P. Solomon, J.Chem.Phys. 62 (1975) 2267
13. K. Hiroaka and P. Kebarle, Nature London, Phys.Sci. 245 (1973) 31
14. M. Fluendy and G. Lawley, Chemical Applications of Molecular Beam Scattering, Wiley & Sons, Inc., New York (1973)

Some years ago we have started this ion cluster investigation, using the slightly modified apparatus of A. van Deursen (ref. 1). With the discovery of the fragmentation of the hydrogen cluster ions upon collision with a gas target, the need for a very intense cluster ion source became urgent. In this thesis, only a trace can be found of the large efforts spent to build this new ion source and to get the whole machine operational with a strong stable ion beam of about 1 μA. As reward we obtained an intensity gain of a factor 10^4 during this work. The stability and energy homogeneity of the ion beam turned out to be very good and are comparable with the same properties for other types of weak ion sources. A recent design of a new type ionizer probably allows to increase the intensity by another factor of 10^2.

In this thesis evidence has been given for the existence of particularly stable hydrogen cluster ions in the mass range up to H_{41}^+, by fragmentation measurements. Based on the experience gained in the course of this work we have constructed a new machine, which shall enable us to extend the mass range up to at least m/e = 10^4 amu. It would be very interesting to obtain information about the stability criteria for these larger hydrogen cluster ions.

In order that all fragment ions arrive at the detector, it looks most favourable to accelerate the fragment ions immediately behind the scattering region to a nearly parallel beam. By variation of the distance between scattering region and the position at which the ions are accelerated, information can be gathered about the angle dependence of the fragmentation cross section. Thus avoiding large angular corrections the stable configurations are more clearly revealed; the energy loss - of which we only could find a slight indication for $H_{15}^+ \rightarrow H_5^+$ - is expected to be much better revealed for

large parent clusters, by the TOF technique.

Except for hydrogen cluster ions, there are many other cluster ion systems which look interesting with respect to stable configurations, e.g. Ar_n^+, K_n^+, He_n^+, or mixed clusters like the theoretically investigated Ar_nK^+.

In case of the present work, the centre of mass energy of the systems was always ample to permit evaporation of all H_2 molecules. By scattering heavy cluster ions against a light scattering partner, this situation becomes different at low energies. Ions can be decelerated to an energy of 1 eV, without great difficulty. The centre of mass energy of the Ar_{20}^+ ion (lab energy 1 eV) colliding with a thermal H_2 amounts to about 0.002 eV; fragmentation will probably not occur. Increasing the energy of the cluster ion we will observe how the fragmentation channels open up one after the other. Information can be obtained about the binding energies e.g. of the argon atoms in the cluster ion Ar_{20}^+, and the threshold behaviour.

References

1. A.P.J. van Deursen, Thesis, Katholieke Universiteit Nijmegen, The Netherlands (1976)

Samenvatting

In dit proefschrift wordt een experimenteel onderzoek naar eigenschappen van waterstof clusterionen botsend met gas moleculen, beschreven. Daartoe worden in een ionenmachine totale en differentiële fragmentatie botsingsdoorsneden gemeten. Voor zover ons bekend is dit het enige onderzoek waarbij met grote clusterionen dit type botsingsexperimenten worden uitgevoerd.

Neutrale waterstof clustermoleculen worden gevormd bij de supersone expansie van tot 30 K gekoeld waterstofgas. Door beschieting van deze clusters met electronen worden de clusterionen gevormd. Deze ionen worden direct na hun ontstaan versneld tot een energie van een paar honderd eV en tot een smalle bundel gefocusseerd. Vervolgens wordt massaselectie toegepast zodat een bundel van wel gedefiniëerde ionen overblijft. De ionen worden vlak voor het verstrooiingscentrum al dan niet afgeremd, doorlopen het verstrooiingsgebied en bereiken tenslotte de detector, waar nogmaals massa analyse van de bundel plaatsvindt.

In hoofdstuk twee zijn de eerste resultaten weergegeven voor de verstrooiing van H^+_{2n+1}; $n \leqslant 13$ tegen stikstof. De energie van de ionen varieert van 250 tot 890 eV. Totale botsingsdoorsneden voor deze clusterionen worden gepresenteerd als functie van de massa en de energie van de ionen. Tevens kon worden aangetoond dat fragmentatie plaatsvindt bij de botsing van een clusterion en een stikstof molecuul. De fragmentionen zelf konden niet gedetecteerd worden.

De ingebruikname van een nieuwe zorgvuldig geoptimaliseerde ionenbron leidde tot een ionenbundel van zeer hoge intensiteit en uitstekende stabiliteit. In hoofdstuk drie en vier zijn de resultaten hiermede verkregen samengevat.

In hoofdstuk drie zijn totale en integrale fragmentatie botsingsdoorsnede metingen weergegeven met H_{2n+1}^+; $n \leq 20$ bundels. Als strooigas werd He gebruikt. De energie van de ionen is gevarieerd tussen 200 en 850 eV. De totale botsingsdoorsnede als functie van de massa van de clusterionen vertoont een strikt lineair gedrag. Geen effect van de afdekking (screening) van H_2 moleculen in de ionen is waargenomen. Als functie van de energie vertoont de totale botsingsdoorsnede een $1/E^s$ gedrag, waarbij s afhankelijk is van de clusterionen massa.

Tevens zijn in hoofdstuk drie de meetresultaten weergegeven van de fragmentatiebotsingsdoorsneden. Deze metingen werden verkregen met een vaste detector invangsthoek van 10^{-4} sterad. De metingen tonen aan dat H_9^+, H_{15}^+, H_{19}^+, H_{23}^+ en H_{27}^+ bijzonder stabiel zijn.

In hoofdstuk vier zijn differentiële botsingsdoorsnede metingen gegeven met H_{2n+1}^+; $n \leq 7$ bundels. Als strooigas werd argon en waterstof gebruikt. De energie van de ionen varieerde tussen 6.8 en 75 eV. Uit deze metingen blijkt dat de hoekafhankelijkheid zowel als de snelheidsafhankelijkheid van de differentiële fragmentatie botsingsdoorsneden op eenvoudige wijze reduceren tot unieke krommen voor elk fragmentatie proces. Een eenvoudig model voor het fragmentatie proces, met als enige parameter de energie van de vrijkomende H_2 moleculen, is voldoende om alle metingen goed te beschrijven. Tevens wordt informatie verkregen over de invloed van de kleine detector opening in hoofdstuk drie op de integrale fragmentatie botsingsdoorsneden.

Curriculum vitae

Op 17 juni 1952 ben ik te Koningsbosch geboren. Na de lagere school volgde ik de middelbare schoolopleiding aan het Bisschoppelijk College St. Jozef te Sittard. Het diploma HBS-B werd behaald in 1969, waarna ik begon met de studie Wis- en Natuurkunde aan de Katholieke Universiteit te Nijmegen. In 1972 werd het kandidaatsexamen cum laude afgelegd, gevolgd door het doctoraalexamen experimentele natuurkunde in 1974. Het experimentele werk voor dit examen werd verricht in de werkgroep Atoom- en Molecuulfysica. Na het doctoraalexamen bleef ik als wetenschappelijk medewerker verbonden aan dezelfde groep. Daar werd onder leiding van Prof.dr. J. Reuss het onderzoek verricht, waarvan de resultaten in dit proefschrift zijn weergegeven. In 1977 werden op uitnodiging van dr. A. Ding, gedurende drie maanden experimenten verricht aan het Hahn-Meitner-Institut te West-Berlijn. De resultaten hiervan zijn eveneens in dit proefschrift opgenomen.
Naast het verrichten van onderzoek werd ook deelgenomen aan de verzorging van het onderwijs. In het kader hiervan heb ik assistentie verleend bij de begeleiding van praktica en werkcolleges.

S T E L L I N G E N

1. Het niet goed kunnen berekenen van polarisatie effecten op de botsingsdoorsneden met behulp van de z.g. coupled state approximatie, is intrinsiek verbonden aan deze benadering.

L. Monchik
J.Chem.Phys. 67 (1977) 4626

2. De chemiluminescentie bij NO + O_3 in "flow tube" experimenten wordt gemeten bij zulke hoge drukken (P ≈ ? mbar), dat sterke botsingsquenching plaatsvindt van het stralende NO_2^* molecuul (P_{quench} ≈ 2×10^{-3} mbar). De effecten, die dit tengevolge kan hebben op de diverse afhankelijkheden van de rate constante, worden ten onrechte buiten beschouwing gelaten.

G.E. Schwartz and H.S. Johnston
J.Chem.Phys. 51 (1969) 1286
R.J. Gordon and M.C. Lin
J.Chem.Phys. 64 (1976) 1058

3. In de beschrijving van de excitatie van een moleculaire bundel door een laser bundel zoals gegeven door Hemminger et al., moet de verbreding van de kortlevende aangeslagen toestand in rekening worden gebracht.

J.C. Hemminger, R. Cavanagh,
J.M. Lisy and W. Klemperer
J.Chem.Phys. 67 (1977) 4953

4. De impliciete aanname gemaakt door T. Amano et al. dat de spindichtheid in het SO-molecuul voor zowel het S als het O atoom aan elkaar gelijk gesteld mag worden, is onjuist.

T. Amano, E. Hirota and Y. Marino
J.Phys.Soc.Jap. 22 (1977) 399
F.D. Wayns and E.A. Colbourn
Mol.Phys. 34 (1977) 1141

5. Uit de door McKellar en Welsh gemeten botsingsgeïnduceerde infrarood absorptie spectra van $(H_2)_2$ dimeren kunnen de relatieve posities van de rotatie niveaus in het dimeer worden bepaald. Men zou deze informatie meer moeten aanwenden als test op ontwikkelde H_2-H_2 potentiaal modellen.

A.R.W. McKellar and H.L. Welsh
Can.J.Phys. 52 (1974) 1082

6. De symbolen gebruikt voor de l-doublingsconstanten van een tweevoudig ontaarde vibratie toestand in een symmetrisch top molecuul zijn niet eenduidig en werken zelfs verwarrend.

J.G. Smith
Mol.Phys. 32 (1976) 621

7. Het optreden van magische getallen beperkt zich niet alleen tot de atoomopbouw, kernopbouw en elementaire deeltjes structuur.

2 november 1978

H.A. van Lumig